



Quantifying the impact of global nitrate aerosol on tropospheric composition fields and its production from lightning NO_x

Ashok K. Luhar¹, Anthony C. Jones², Jonathan M. Wilkinson^{2,a}

5 ¹CSIRO Environment, Aspendale, Victoria 3195, Australia

²Met Office, Fitzroy Road, Exeter, EX1 3PB, UK

^anow at: Forecast Department, European Centre for Medium-Range Weather Forecasts, Reading, UK

10 *Correspondence to:* Ashok K. Luhar (ashok.luhar@csiro.au)

Abstract. Several global modelling studies have previously studied the effects of lightning-generated oxides of nitrogen (LNO_x) on gas-phase chemistry and atmospheric radiative transfer. However, there has been limited attention on quantifying the role of LNO_x production on aerosol, particularly when nitrate aerosol is included. In the present paper, we address two questions: 1) what is the impact of including nitrate aerosol on tropospheric composition fields, aerosol optical depth (AOD) and radiation, and 2) what is the dependency of these impacts on the lightning parameterisation and the amount of LNO_x ? For this purpose, we use the Met Office's Unified Model (UM) – United Kingdom Chemistry and Aerosol (UKCA) global chemistry-climate model, which now includes a nitrate scheme in its modal aerosol component, alongside two empirical lightning flash-rate parameterisations. We find that both nitrate aerosol and changes in LNO_x lead to significant changes in tropospheric composition and aerosol responses. For instance, with the inclusion of nitrate aerosol, the tropospheric ozone burden decreases by approximately 4–5%, while the tropospheric methane lifetime increases by a similar degree. For an increase of 5.2 Tg N yr^{-1} in LNO_x from a baseline of zero, there is a global mean enhancement of 2.8% in NH_4 , 4.7% in fine NO_3 , 12% in coarse NO_3 , and 5.8% in SO_4 aerosol mass burdens, indicating that LNO_x impacts coarse aerosol the most comparatively. The inclusion of nitrate aerosol affects the aerosol size distribution too, with the most significant changes occurring in the Aitken and accumulation modes. As LNO_x increases, the mean global AOD and top-of-atmosphere net downward radiative flux also increase (the latter being more influenced by tropospheric ozone increases), whereas nitrate aerosol causes a change of -0.4 W m^{-2} in this radiative flux in our simulations. The results presented in this paper when considered in the context of the large uncertainty in the global amount of LNO_x suggest that there could be bigger variations in the values of the atmospheric parameters considered.



30 **1 Introduction**

Liquid or solid particles in the atmosphere, called aerosols, have a considerable impact on Earth's energy budget and thus the climate system, and also impact air quality. Aerosols can be emitted directly from both anthropogenic and natural sources (termed primary aerosols), or they can be chemically produced in the atmosphere from precursor gases by condensation of vapours on pre-existing particles or by nucleation of new particles (termed secondary aerosols). Although atmospheric
35 aerosol can comprise many different species, the main groups include sulfate (SO_4^{2-} , or simply SO_4), nitrate (NO_3^- , or simply NO_3), ammonium (NH_4^+ , or simply NH_4), carbonaceous aerosols (e.g., organic carbon and black carbon), sea salt, and mineral dust, with their sizes varying from nanometres to tens of micrometres dependent on the formation process (Szopa et al., 2021). Apart from exerting a direct radiative forcing (i.e. a change in the energy budget at the top of atmosphere (TOA)), aerosols also impact clouds through aerosol–cloud interactions which in turn impact radiative forcing indirectly.

40 Sulfate and nitrate are predominantly secondary inorganic aerosols produced from atmospheric oxidation and are often the major components of fine mode aerosol (Haywood and Boucher, 2000). They are strong scatterers of the incoming solar energy (the 'aerosol direct effect') and thus exert a negative radiative forcing on climate (meaning a cooling of the atmosphere). These aerosols also act as the cloud condensation nuclei (CCN), and modify cloud properties, such as cloud albedo, persistence or lifetime of clouds and precipitation rate (the 'aerosol indirect effect').

45 Sulfate is formed by oxidation of precursor sulfur dioxide (SO_2) in gas phase and in aqueous phase in cloud droplets. The main precursor species for the chemical formation of nitrate aerosol are reactive gases of nitric acid (HNO_3) and ammonia (NH_3). HNO_3 is the oxidation production product of nitrogen oxides (NO_x). NO_x is a mixture of nitric oxide (NO) and nitrogen dioxide (NO_2), and it is primarily emitted from anthropogenic burning of fossil fuel and from natural sources, such as biomass burning, soil emissions, and lightning. It is also an important air pollutant by itself, and further impacts air
50 pollution and radiation, for example, through net tropospheric ozone (O_3) production and changes in tropospheric methane lifetime caused by changes in the hydroxyl radical (OH). Major emissions of NH_3 gas include agricultural sources, which include volatilisation of livestock manure and mineral fertiliser application. Sulfate aerosol also indirectly influences nitrate aerosol and O_3 levels through changes in oxidation rates and by eroding ammonia concentrations.

Sulfate and nitrate particles (or in particles) can be dry or in aqueous solution and their production takes place through
55 complex chemical pathways (Finlayson-Pitts and Pitts, 2000). In short, SO_2 and NO_x are oxidised into sulfuric acid (H_2SO_4) (liquid aerosol droplets) and HNO_3 (atmospheric gas), respectively. H_2SO_4 reacts with NH_3 to produce aerosol of ammonium sulfate (NH_4HSO_4 and $(\text{NH}_4)_2\text{SO}_4$). Thus, tropospheric sulfate aerosol may be considered as consisting of sulfuric acid particles that are partially or totally neutralised by NH_3 . After H_2SO_4 is neutralized, any excess NH_3 then combines with HNO_3 to form aerosol of ammonium nitrate (NH_4NO_3). Low temperature, high relative humidity, and elevated fine
60 particulate matter favour nitrate production (Szopa et al., 2021; references therein).



Ammonium and nitrate aerosols formed through these gas-to-particle reactions are a large portion of fine-mode particles (with a diameter $< 1\mu\text{m}$) affecting both climate and air quality, particularly over populous regions in the Northern Hemisphere (Szopa et al., 2021). In addition to fine mode, coarse-mode nitrate aerosol is formed when HNO_3 condenses irreversibly onto existing sea-salt and dust aerosols to produce sodium nitrate (NaNO_3) and calcium nitrate ($\text{Ca}(\text{NO}_3)_2$) salts, respectively (Li and Shao, 2009). The coarse-mode nitrate aerosol dominates the global mass burden of nitrate, which may be important from air quality side, but has little radiative effect in the solar spectrum compared to the fine-mode nitrate (Bian et al., 2017; Hauglustaine et al., 2014).

Apart from its direct effects on climate and air quality, nitrate aerosol through its deposition also plays a part in constraining net primary productivity, thus altering sequestration of carbon and ecological effects (Bian et al., 2017). Nitrate aerosol is expected to become even more important in the future atmosphere due to the continued increase in nitrate precursor emissions (e.g., NH_3 and NO_x) and the decline in SO_2 due to stricter emissions regulations (Bellouin et al., 2011; Hauglustaine et al., 2014). For example, this could be due to increasing use of ammonia based fertilisers and the potential use of ammonia as an effective medium for storing and transporting hydrogen as a fuel in a competitive net zero carbon economy. Despite the above, few global chemistry-climate models include nitrate aerosol, and usually its effects are completely ignored (Tost, 2017), with the main reason being the chemical complexity of nitrate formation and the semi-volatile nature of ammonium nitrate. To give an example, of the ten global Earth system models that participated in the Aerosol and Chemistry Model Intercomparison Project (AerChemMIP) of the Coupled Model Intercomparison Project Phase 6 (CMIP6), aimed at understanding the effects of reactive gases and aerosols on Earth's climate, only two had an interactive stratospheric and tropospheric gas-phase and aerosol-chemistry scheme together with an explicit treatment of nitrate aerosol (Thornhill et al., 2021) and both models used a single-moment aerosol approach in which aerosol component mass is a prognostic variable.

As mentioned above, lightning is a major source of NO_x , particularly in the tropical to subtropical middle to upper troposphere where lightning is mostly discharged (Murray, 2016; Bucsela et al., 2019). Although lightning-generated NO_x (abbreviated as LNO_x) constitutes only about 10% of the total NO_x source emissions globally, it has an inordinately large effect on tropospheric composition (e.g., Murray, 2016; Luhar et al., 2021), such as the OH and O_3 mixing ratios. To give an example, whilst NO_x emissions from lightning are similar in magnitude to those from soils or biomass burning, they contribute about three times as much to the total tropospheric O_3 column due to conducive atmospheric conditions in regions where the bulk of LNO_x is released (Dahlmann et al., 2011).

Previous global modelling studies have demonstrated the importance of LNO_x on atmospheric gas-phase chemistry and oxidation capacity (see for example, Labrador et al., 2005, Schumann and Huntrieser, 2007; Finney et al., 2016; Gressent et al., 2016; Gordillo-Vázquez et al., 2019, and Luhar et al., 2021), and also its impact on cloud cover and atmospheric radiative transfer (e.g., Luhar et al., 2022). Even though these modelling studies did not explicitly include nitrate aerosol processes, an indirect impact of LNO_x on aerosol is implicit through perturbations to the oxidation capacity of the



atmosphere (e.g. via changes in OH and O₃), for example enhancement of new particle formation and aerosol abundances
95 stemming from faster oxidation rates of gas-phase sulfur to sulfate (Murray, 2016; Tost, 2017; Luhar et al., 2022).

The area of quantifying the role of LNO_x production on aerosol, particularly with nitrate aerosol included, has only received very limited attention (e.g., Tost, 2017) compared to its role on gaseous atmospheric composition, possibly because, as mentioned earlier, the chemical complexity of nitrate formation and the semi-volatile nature of ammonium nitrate (whereby a considerable part of it reevaporates in the atmosphere (e.g., Stelson et al., 1979)). Chemical conversion of LNO_x into HNO₃
100 is more favourable in the middle to upper troposphere, where lightning NO_x mostly occurs, as compared to within the atmospheric boundary layer due to differences in chemical composition, chemical reactivity, and loss processes (Tost, 2017). Tost (2017) points to observational support for the occurrence of both NH₃ and NO₃ aerosol in convective outflows so that the formation of NH₄NO₃ is likely because of the low temperatures in the upper troposphere.

The global modelling study by Tost (2017), which involves a modal aerosol scheme with nitrate included, is possibly the
105 only modelling study to show that LNO_x (parameterised via the Price and Rind (1992) (PR92) scheme described below) is an significant source of nitrate in the upper troposphere and influences the aerosol size distribution and radiation. A more comprehensive study involving the sensitivity of tropospheric composition (including aerosol) to global lightning parameterisation with and without nitrate is currently lacking and the present paper aims to address that. Recently, a nitrate scheme has been included in the modal aerosol scheme of the Met Office's Unified Model (UM) – United Kingdom
110 Chemistry and Aerosol (UKCA) global chemistry-climate model, hereafter denoted UM-GA8.0-UKCA or UM-UKCA, where GA8.0 refers to the configuration of the Global Atmosphere in the UM (Jones et al., 2021). The aerosol scheme in UM-UKCA is a prognostic double-moment scheme (Mann et al., 2010) which transports both particle number and mass concentrations in size classes. In this paper, we apply UM-UKCA to study the sensitivity of tropospheric composition and radiation to the lightning parameterisation with and without nitrate aerosol included.

115 Ultimately, the questions we seek to answer using UM-UKCA are: 1) what is the impact of adding nitrate to UM-UKCA on tropospheric composition fields (such as O₃, OH, NO_x, methane lifetime, and aerosol), AOD and radiation, and 2) what is the dependency of these impacts on the lightning parameterisation in the model? For this purpose, we apply UM-UKCA without and with nitrate and vary LNO_x through the use two empirical parameterisations of lightning flash rate: (a) the PR92 parameterisations for ocean and land which are a function of convective cloud-top height and which most global chemistry-
120 climate models use (Tost, 2017; Archibald et al., 2020), and (b) Luhar et al.'s (2021) (termed Lu21) flash-rate parameterisations which improve upon the PR92 parameterisation for the ocean. Simulations are also conducted with no LNO_x. An outline of the paper is as follows. In Section 2, we provide details of the LNO_x parameterisations used; Section 3 briefly describes the global UM-UKCA model configuration used, with some extra detail about model's aerosol scheme with nitrate and the model simulation setup; this is followed by results and discussion and then conclusions.



125 2 Lightning-generated NO_x parameterisations

In traditional lightning parameterisations used in general circulation models, the amount of LNO_x is estimated as

$$LNO_x = P_{NO} \times F, \quad (1)$$

where P_{NO} is the amount of NO produced per flash. The flash rate F is computed for every model time step and each grid column.

130 In global chemical transport and chemistry-climate models (including most CMIP6 models), F (flashes per minute) is most commonly parameterised in terms of convective cloud-top height using Price and Rind's (1992) (PR92) formulas for land (F_L) and ocean (F_O) as follows:

$$F_L = 3.44 \times 10^{-5} H^{4.9}, \quad (2)$$

$$F_O = 6.4 \times 10^{-4} H^{1.73}, \quad (3)$$

where the convective cloud-top height (H , in km) is supplied by the convection scheme of the model. The oceanic flash rates obtained from Eq. (3) are about 2 to 3 orders of magnitude smaller as compared to those computed using Eq. (2) for overland clouds.

135 The calculated flash rate (F_L or F_O) is divided into intracloud (IC) and cloud-to-ground (CG) components, F_{IC} and F_{CG} , and respective emission factors for the amount of NO released per IC and CG flash, $P_{NO,IC}$ and $P_{NO,CG}$, are applied, i.e.,

$$LNO_x = P_{NO,IC} \times F_{IC} + P_{NO,CG} \times F_{CG}. \quad (4)$$

The calculated amount of NO is then non-linearly distributed in the vertical in the grid column (e.g., Luhar et al., 2021).

140 Eq. (3) is known to greatly underpredict flash rates over the ocean. Luhar et al. (2021) tested the PR92 flash-rate formulas in the Australian Community Climate and Earth System Simulator – UKCA (or ACCESS-UKCA) global chemistry-climate model without nitrate aerosol (which is essentially UM-UKCA with the UM at vn8.4) using satellite based lightning data and concluded that whilst the PR92 formula for land (Eq. (2)) performs satisfactorily, the oceanic formula, Eq. (3), predicts a mean global flash rate that is smaller by a factor of approximately 30 compared to the observed, thus results in a proportional underestimation of LNO_x over the ocean.

145 Luhar et al. (2021) formulated the following updated flash-rate parameterisations following the scaling relationships between thunderstorm electrical generator power and storm geometry developed by Boccippio (2002), coupled with available data:

$$F_L = 2.40 \times 10^{-5} H^{5.09}, \quad (5)$$

$$F_O = 2.0 \times 10^{-5} H^{4.38}. \quad (6)$$



In the study by Luhar et al. (2021), Eq. (5) did very similar to Eq. (2) in estimating the spatial pattern of the global continental lightning flash rate, giving a global mean value of 35.9 flashes s^{-1} compared to the satellite climatological value of 38.5 flashes s^{-1} . The updated oceanic parameterisation (6) simulated the oceanic (and thus the total $F = F_L + F_O$) flash-rate data much better, giving a mean global oceanic flash rate of 9.1 flashes s^{-1} compared to 7.7 flashes s^{-1} derived from the satellite climatology. However, there was still an underestimation of flash frequencies in the extratropics, which is probably an inherent limitation of the convective cloud-top height approach to parameterise F . The updated flash-rate parameterisations resulted in an increase in the global LNO_x by ~ 40% (from the default value of 4.8 Tg N yr⁻¹), causing a significant change on the tropospheric composition compared to the default model run.

There is a large uncertainty in the global LNO_x amounts. For example, Schumann and Huntrieser (2007) cite an uncertainty of 2–8 Tg N yr⁻¹. Other estimates include 4–8 Tg N yr⁻¹ (Martin et al., 2007), and ~ 9.0 Tg N yr⁻¹ (Nault et al., 2017). The range of global LNO_x in five CMIP6 Earth system models for the present-day conditions ranged 3.2–7.6 Tg N yr⁻¹ (Griffiths et al., 2021; Szopa et al., 2021). A major reason for this is due to the poor constraining of the quantity of NO produced per flash. The default in the UM-UKCA model, as used by Luhar et al. (2021), is $P_{NO,IC} = P_{NO,CG} = P_{NO} = S_f \times 10^{26}$ molecules of NO produced per flash, where it is assumed that the scaling factor $S_f = 2$. This is equal to $P_{NO} = 330$ moles NO produced per flash, which is close to the middle of the large range 70–665 moles NO per flash reported in the scientific literature based on observations (Luhar et al., 2021). Here, we use $S_f = 1.7$, so $P_{NO} = 280$ moles NO per flash, which can be compared with 280 ± 80 moles NO produced per flash obtained by Marais et al. (2018) using satellite-based lightning data and the Ozone Monitoring Instrument (OMI) NO₂ columns coupled with the GEOS-Chem global chemical transport model, and 310 moles NO per flash suggested by Miyazaki et al. (2014) based on an assimilation into a global CTM of satellite observations of atmospheric composition and flash distribution.

Because P_{NO} is taken independent IC and CG in our model, the partitioning of flash rate into the IC and CG flash rates only affect the shape of the vertical profile of LNO_x distribution. The total amount of LNO_x released remains independent of this partitioning.

3 The Met Office Unified Model (UM) with global chemistry and aerosol

We use the Met Office Unified Model (UM) which includes global atmosphere and coupled modelling systems from weather to climate timescales. The latest available release (at the time) of the UM (vn13.2) involving the science configurations Global Atmosphere vn8.0 (GA8.0) and Global Land vn9.0 (GL9.0) configuration of the Joint UK Land Environment Simulator (JULES) land surface model was selected. (The new nitrate aerosol scheme was included in the UM at UM vn11.8 (Jones et al., 2021) with the corresponding science configurations GA7.1 and GL7.0 as described by Walters et al. (2019) and updates between GA7.0 and GA8.0 pertinent to aerosols described in Jones et al. (2022)).



The horizontal resolution of the model is 1.875° longitude \times 1.25° latitude and there are 85 staggered hybrid-height levels which extend from the surface to 85 km in the vertical (the so-called N96L85 climate configuration). The resolution in the vertical becomes coarser, with the lowest 50 levels under 18 km altitude. The model was run in atmosphere-only mode with a dynamical timestep of 20 min. Monthly climatologies of sea surface temperature and sea ice fields for the year 2000 are prescribed, which are generated by averaging over the 1995–2004 time series data created for CMIP6 atmosphere-only model simulations. This is the same model setup as Jones et al (2021), albeit using the GA8.0 rather than GA7.1 atmosphere model.

Atmospheric composition in the UM is described by the United Kingdom Aerosol and Chemistry (UKCA) model (<https://www.ukca.ac.uk>), with model's chemical solver called every 60 min. The UKCA configuration used here employs a combined stratosphere–troposphere chemistry scheme (namely, StratTrop1.0) (Archibald et al., 2020), which also contains the multi-modal, multi-component, double-moment GLObal Model of Aerosol Processes (GLOMAP)-mode aerosol microphysics scheme as described by Mann et al. (2010) and Mulcahy et al. (2020). GLOMAP-mode as coupled to UKCA chemistry is termed UKCA-mode.

With 84 species and 291 chemical reactions, the StratTrop1.0 scheme in UKCA simulates the chemical cycles of O_x , HO_x , NO_x , and halogenic compounds; the oxidation of carbon monoxide (CO), methane (CH_4) and other volatile organic compounds (VOCs); and heterogenous chemistry on Polar Stratospheric Cloud and tropospheric aerosols. The Fast-JX scheme (see Telford et al., 2013) is used to model interactive photolysis. Gaseous wet and dry deposition are included.

Atmospheric radiative transfer is described via a two-stream approximation, with 9 longwave bands and 6 shortwave bands (Manners et al., 2023). The Prognostic Cloud fraction and Prognostic Condensate (PC2) scheme is used to model large-scale cloud (Wilson et al., 2008) and cloud microphysics is simulated using a single-moment scheme (Wilson and Ballard, 1999) with extensive revisions (as included in GA8.0). The radiation changes include both direct aerosol radiative forcing and indirect radiative effects of clouds and atmospheric composition changes. The convection scheme is based on a mass flux-approach (Gregory and Rowntree, 1990) with several extensions to include convective momentum transport and downdrafts (Walters et al., 2019).

The full modelling system we use is termed UM-GA8.0GL9.0-UKCA, which in this paper is referred to as UM-UKCA.

3.1 UKCA-mode aerosol scheme with nitrate

UKCA-mode as used here is a double-moment aerosol microphysics scheme that transports aerosol number and mass concentrations in lognormal size modes (four soluble and one insoluble) (Mann et al., 2010; Mulcahy et al., 2020). This is the default UKCA-mode setup 2 (see Table 1). For each mode, the median aerosol dry radius is allowed to evolve within specified size ranges, but the lognormal standard deviation (i.e. “mode width”) is kept fixed. This scheme thus resolves the differential growth of particles and their composition across the aerosol size range including internal mixtures. The default UKCA-mode configuration involves sulfate (SO_4), organic matter (OM), black carbon (BC) and sea salt (SS). Species in



each mode are considered as an internal mixture. On the other hand, mineral dust is treated outside of UKCA-mode and is represented by a six-bin scheme developed as part of the older single-moment Coupled Large-scale Aerosol Simulator for
210 Studies in Climate (CLASSIC) framework (Woodward et al., 2001; Bellouin et al., 2013).

With the new nitrate scheme (Jones et al., 2021), ammonium (NH_4), nitrate (NO_3), and coarse nitrate (denoted coarse NO_3) are added to the standard aerosols, namely SO_4 , OM, BC and SS, and the new UKCA-mode setup consists of 28 aerosol tracers (23 mass + 5 number concentrations) in total (Table 1) (the UKCA-mode setup 10). Note that here “ NO_3 ” refers exclusively to semi-volatile NO_3 linked with NH_4 , whereas “coarse NO_3 ” pertains to stable NO_3 related to sea salt and dust.
215 NH_4 and NO_3 mass is introduced into the Aitken soluble and accumulation soluble modes and it may be moved to the coarse soluble mode through aerosol processing, whereas coarse NO_3 is restricted to the accumulation soluble and coarse soluble modes. Only nitrate condensing on bins 2-6 (i.e., accumulation and coarse modes) of the mineral dust scheme is considered. The nitrate scheme requires NH_3 and HNO_3 to be available (emission of NH_3 is prescribed, while gaseous HNO_3 is produced by various chemical reactions in the atmosphere). Full detail of the methodology is reported by Jones et al. (2021).

220 The component of the new nitrate scheme dealing with the formation of fine-mode NH_4NO_3 from the condensation of HNO_3 and NH_3 is numerically solved first, prior to the condensation of HNO_3 on coarse aerosols (i.e., dust and sea salt). This fine-mode component is a quasi-instantaneous thermodynamic equilibrium scheme, which, in contrast to commonly utilised “instantaneous” thermodynamic equilibrium nitrate schemes, restricts the rate at which NH_4NO_3 levels attain equilibrium by utilising Schwartz’s (1986) first-order uptake theory and applying Fuchs and Sutugin’s (1970) correction factors for
225 molecular effects and for limitations in interfacial mass transport.

Jones et al. (2021) tested the sensitivity of NH_4NO_3 levels to the HNO_3 condensation or uptake rate coefficient (γ) (a key parameter in the first-order uptake theory), with two values $\gamma = 0.193$ and 0.001 (selected from the literature) to represent fast and slow uptake rates, respectively. They found that, generally, the fast uptake value shows a higher spatial correlation with measured nitrate surface concentrations whereas the slow value simulates their magnitudes better. In this study, we use the
230 FAST value $\gamma = 0.193$, which is currently default in UKCA-mode and which may represent the upper end of efficiency of NH_4 and NO_3 production and its impact in the UM. However, Jones et al. (2021) recognised that rather than being globally invariant, γ may vary with aerosol composition, temperature, and relative humidity, and needs better constraining, thus needing further research and future model development outside the scope of the present study.

The model’s radiation scheme and treatment of hygroscopic growth has been modified to include the direct radiative effects
235 of nitrate aerosol and the indirect impacts on clouds, enabling a comprehensive nitrate impacts assessment in future UM studies (Jones et al., 2021).



240 **Table 1: Aerosol size distribution used in the UKCA-mode aerosol scheme. Species are sulfate (SO₄), black carbon (BC), organic matter (OM), sea salt (SS), ammonium (NH₄), nitrate (NO₃), and coarse nitrate (coarseNO₃) (adapted from Jones et al. (2021)).**

Aerosol mode	Geometric mean diameter (nm)	Geometric standard deviation	Species in the standard aerosol scheme	Additional species with nitrate scheme
Nucleation soluble	1–10	1.59	SO ₄ , OM	-
Aitken soluble	10–100	1.59	SO ₄ , BC, OM	NH ₄ , NO ₃
Accumulation soluble	100–1000	1.4	SO ₄ , BC, OM, SS	NH ₄ , NO ₃ , coarseNO ₃
Coarse soluble	> 1000	2.0	SO ₄ , BC, OM, SS	NH ₄ , NO ₃ , coarseNO ₃
Aitken insoluble	10–100	1.59	BC, OM	-

3.2 Model simulation setup

We conducted six UM-UKCA simulations for various combinations of the LNO_x and nitrate schemes, including no nitrate and no LNO_x cases (Table 2). The model experimental setup is very similar to that by Jones et al. (2021). All simulations are initialised with results from a previously spun-up model experiment and are run for model years (1989–2008). To further eliminate any spin-up effects, model output from only the last 15 years (1994–2008) is used for analysis. The model is forced by prescribed sea-surface temperature and sea-ice fields specified as monthly varying climatologies for the ‘year 2000’, which are essentially averages over the 1995–2004 timeseries data developed for CMIP6 atmosphere-only simulations. No meteorological nudging is used so as to allow feedback mechanisms to create an individual climate state. The use of perpetual year 2000 conditions in our simulation design follows standard simulation protocol for the development of the UKCA model in the Met Office. For a statistical robustness of the included feedbacks in the model, instead of examining individual years of the simulations, we present results that are averages over the 15-yr simulation period.

The gaseous and aerosol emissions are mainly prescribed from the CMIP6 historical emissions inventory as monthly fields and they include anthropogenic, biomass burning and natural categories. Jones et al. (2021) provide further details on these emissions including global total for each UKCA chemical species. In our simulations, monthly emissions for the year 2000, which are generated by averaging over the 1995–2004 timeseries data, are used and the emissions are computed every model time step of 20 min. The only extra species emission used by the model when the nitrate scheme is invoked is that of NH₃, whose global total was 53.5 Tg N yr⁻¹, of which 78% was from anthropogenic sources, 15% from the ocean, and 7% from biomass burning.

260 The global total NO_x emission (excluding LNO_x) was 49.6.3 Tg N yr⁻¹, of which the soil, anthropogenic surface, biomass burning, and aircraft components were 11, 72.5, 15 and 1.5%, respectively. Note that the LNO_x emission is not included in the input emissions database and is generated interactively as described in Section 2.



Concentrations of long-lived species CO₂, CH₄, N₂O and O₃ depleting substances are prescribed as lower boundary conditions at the surface (Archibald et al., 2020). All simulations used the optional two-layered oceanic process-based scheme proposed by Luhar et al. (2018) (configuration corresponding to the Ranking 1 in their Table one) for dry deposition ozone to the ocean.

Table 2: Details of six UM-UKCA simulations performed in this study. The indicated lightning schemes are Price and Rind (1992) (PR92) and Luhar et al. (2021) (Lu21). The uncertainty corresponds to a 1-sigma standard deviation calculated from annual means over 15 years of simulation (sample size = 15).

Simulation name	Nitrate status	Lightning scheme	Global LNO _x (Tg N yr ⁻¹)	Tropospheric methane lifetime (yr)	Tropospheric O ₃ burden (Tg)
NN_0	No nitrate	-	0	8.55 ± 0.03	278.5 ± 2.2
NN_PR	No nitrate	PR92	3.41	7.49 ± 0.03	325.2 ± 3.5
NN_Lu	No nitrate	Lu21	5.24	7.03 ± 0.02	348.8 ± 3.0
WN_0	With nitrate	-	0	9.15 ± 0.04	260.8 ± 3.4
WN_PR	With nitrate	PR92	3.36	7.90 ± 0.03	307.1 ± 2.3
WN_Lu	With nitrate	Lu21	5.18	7.38 ± 0.02	332.6 ± 2.5

270 4 Results and discussion

In the following section, we present the impact of LNO_x on tropospheric composition and radiation with and without nitrate aerosol.

4.1 Modelled lightning flash rate and LNO_x

Luhar et al. (2021) previously evaluated the flash-rate parameterisations Eq. (2) – (6) within their ACCESS-UKCA model (which is UM-UKCA vn8.4 (with GA4.0) and which does not have nitrate aerosol) using the Lightning Imaging Sensor (LIS) / Optical Transient Detector (OTD) satellite data of global flash-rate distribution (Cecil et al., 2014). Here, we have used the above flash-rate parameterisations in UM-UKCA at vn13.2 (with GA8.0), both with and without nitrate – this model version has essentially the same convection scheme as in vn8.4 and therefore results in similar global flash-rate distributions. Here, we only do a limited comparison of the simulated flash-rate density with the LIS/OTD climatology since a comprehensive evaluation (including a seasonal comparison) has already been done by Luhar et al. (2021).

The LIS/OTD flash density climatology in Figure 1a shows high overland values in the tropics and subtropics, as well as in lower midlatitudes. Some relatively high levels are also observed over water at these latitudes, especially over the western Atlantic, Pacific, western Indian Ocean close to southern Africa, and the waters around the maritime continent. The modelled flash density distribution in Figure 1b obtained using the PR92 scheme is able to reproduce the broad observed



285 distribution at low latitudes over land (barring parts of India), however, it is apparent that it does not simulate well the
extension of the observed flash density over the temperate latitudes, especially in the Northern Hemisphere. It is also clear
that the PR92 scheme predicts nearly zero marine flash density, contrary to the observations. On the other hand, the Lu21
scheme reproduces the observed distribution of lightning flash density over the ocean considerably better compared to the
PR92 scheme (Figure 1b), although some significant spatial differences are visible (for example, high bias over the Pacific
290 and equatorial Indian Ocean, and the low bias over western Indian Ocean close to southern Africa) compared to the
LIS/OTD climatology. The simulated overland distributions in Figure 1b and Figure 1c are very similar.

The simulated flash-rate distributions in Figure 1b and Figure 1c show a few small areas with relatively high flash-rate in the
western equatorial Pacific Ocean (i.e., mostly areas east of the Philippines), and this is most likely because the land-sea mask
used at N96 resolution in the present model to distinguish between land and ocean for flash-rate calculation treat these grid
295 point areas as land. Noting that there do not seem to be corresponding high flash-rate spots in the observations (Figure 1a),
we recommend in future versions of UM-UKCA that these grid points be treated as water in the land-sea mask (or
alternatively a minimum land fraction threshold for lightning onset could be applied).

With the present UM-UKCA, the total global lightning flash frequency obtained from the PR92 scheme without nitrate is
27.7 flashes s^{-1} , of which 27.2 flashes s^{-1} is over the land and 0.5 flashes s^{-1} is over the ocean. The corresponding values for
300 the Lu21 scheme are 42.5, 30.9 and 11.6 flashes s^{-1} . For comparison, the values obtained from the LIS/OTD climatology are
46.3, 38.5 and 7.7 flashes s^{-1} (Cecil et al., 2014; Luhar et al., 2021), respectively, which show a considerable improvement in
the flash-rate estimate by the Lu21 scheme over the ocean. In the study by Luhar et al. (2021) using UM at vn8.4, the same
PR92 scheme yielded 32.9, 32.5 and 0.4 flashes s^{-1} , respectively, and the same Lu21 scheme yielded 45.0, 35.9 and 9.1
flashes s^{-1} , respectively. These differences in the flash rate between the two model versions show the impact of incremental
305 changes made in the model, although the approach used in the convection scheme remains the same in both model versions.

When nitrate is explicitly added to the model, the PR92 scheme gives 27.3 flashes s^{-1} and the Lu21 scheme gives 42.0
flashes s^{-1} for the globe. Therefore, there is a very small decrease ($\sim 1.3\%$) in flash frequency for both PR92 and Lu21
schemes with nitrate in UM-UKCA, which demonstrates how inclusion of nitrate aerosol may influence lightning flash rate
itself. While this is interesting, we have not investigated this further given that these are atmospheric-only simulations and
310 ocean feedbacks may change the impact of nitrate on flash rate. Note that this nitrate-lightning feedback may be due to
indirect effects of nitrate aerosol through cloud microphysics and radiation that impact model's meteorology and convection
scheme (note also that there is a high sensitivity of the parameterised flash rate to cloud-top height due to its almost 5th
power dependence on the latter, so even minute variations in cloud-top height can cause significant changes in the calculated
flash rate). In this context, there is some work done by Wang et al. (2018) on the effects of aerosols on NO_x production by
315 lightning via direct and indirect aerosol effects.

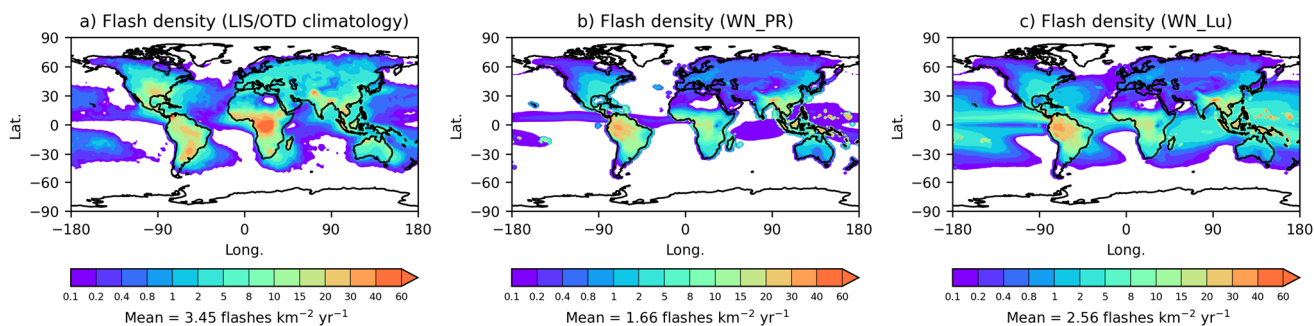


Figure 1: Global distribution of the mean lightning flash density (flashes $\text{km}^{-2} \text{yr}^{-1}$): (a) the LIS/OTD satellite climatology, (b) the modelled distribution using the PR92 flash-rate parameterisations, and (c) modelled distribution using the Lu21 flash-rate parameterisations (both with nitrate aerosol included).

320

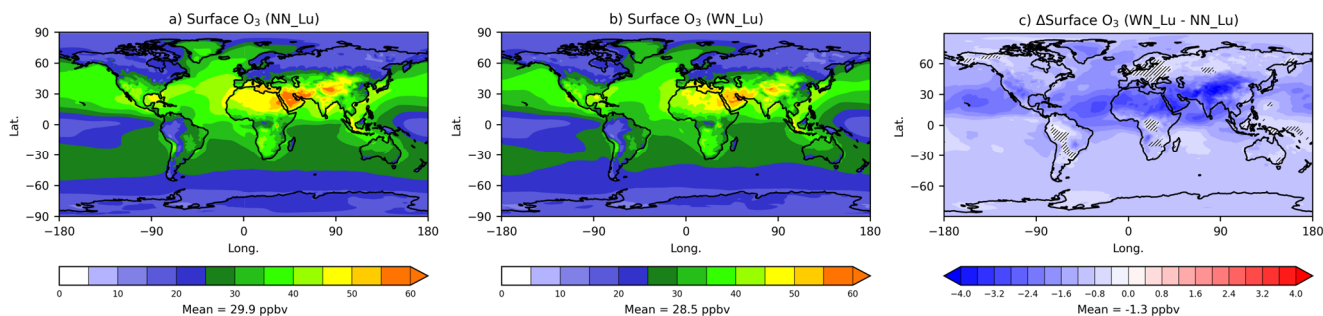
Since P_{NO} has a fixed value, the above differences in the modelled flash rate are reflected in nearly linear proportion in the global LNO_x amounts obtained from the various model runs (see Table 2).

4.2 Impact of nitrate aerosol on gas-phase tropospheric composition

325 The importance of LNO_x on gas-phase tropospheric composition has previously been demonstrated by several studies (e.g., Labrador et al., 2005, Gordillo-Vázquez et al., 2019, and Luhar et al., 2021). Below, we examine the impact of inclusion of nitrate on the modelled gas-phase tropospheric composition, viz. total O_3 , NO_x , OH and CO and methane lifetime, by considering the ‘no-nitrate’ (NN_Lu) and ‘with-nitrate’ (WN_Lu) runs involving the Lu21 flash-rate parameterisation.

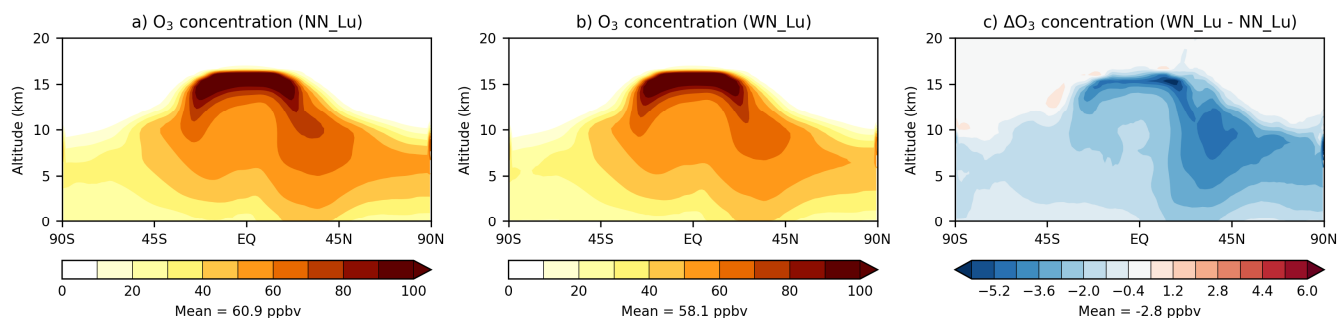
330 The modelled near-surface (at the lowest 20-m model level) O_3 mixing ratio (ppbv) distribution in Figure 2a and b suggests that both NN_Lu and WN_Lu cases look qualitatively very similar, showing relatively high levels in the Northern Hemisphere, particularly within $0-50^\circ N$ which can be associated with the higher precursor emissions in these regions. However, it is apparent from the difference plot (Figure 2c) that there is a global decrease of near-surface O_3 when nitrate is included. This decrease is as much as 3 ppbv within the above latitudinal region, and on-average it is 4.3% (from the global mean of 29.9 ppbv). Figure 2c also displays areas of statistically insignificant difference (defined as significance level less than 5%) which suggest that the differences are significant over most of the globe.

335



340 **Figure 2: Near-surface ozone concentration (ppbv) modelled (a) without (NN_Lu) and (b) with (WN_Lu) the nitrate scheme. The difference (WN_Lu - NN_Lu) is shown in (c). The Lu21 lightning flash-rate parameterisation was used. The difference plot (c) also shows hatched areas representing statistically insignificant difference (significance level less than 5%).**

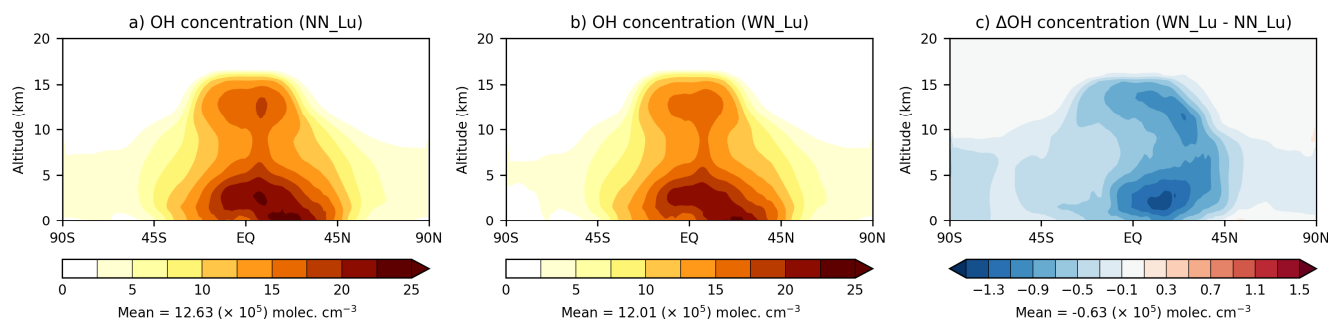
In the model, the tropopause is defined as follows. In the extratropics (latitude $\geq |28|^\circ$), the tropopause is the pressure level of the 2-PVU (potential vorticity units) surface, and in the tropics (latitude $\leq |13|^\circ$) it is the pressure level of the 380 K potential temperature isentropic surface. Between the two latitudes, a weighted average of the two definitions is used following the method of Hoerling et al. (1993). The zonal mean tropospheric O_3 from the two runs also look very similar qualitatively (Figure 3a and b) with less O_3 in the lower troposphere (altitudes < 5 km) over the Southern Hemisphere compared to that over the Northern Hemisphere. Inclusion of nitrate results in O_3 decreases throughout the troposphere (Figure 3c) with the biggest decreases being located in the mid to upper troposphere in the Northern Hemisphere. The volume-weighted global mean tropospheric O_3 obtained with nitrate is 58.1 ppbv which is 4.6% lower than with no nitrate. Similarly, the tropospheric ozone burden decreases by the same relative amount (by 16 Tg from 348.8 Tg to 332.8 Tg) with nitrate (see Table 2). Recently, an evaluation study by Russo et al. (2023) involving UM-UKCA (without nitrate) and focusing on the North Atlantic region suggests a considerable model positive bias for ozone in the tropical upper troposphere. They attribute this to shortcomings of the model's convection and lightning parameterisations (the latter based on the convective cloud-top height approach), which underestimate lightning flashes in mid-latitudes relative to the tropics, which was also evident in the study by Luhar et al. (2021). However, it is clear from Figure 3c that the inclusion of nitrate in the model may alleviate model's positive ozone bias in the tropical upper troposphere to some extent.



360 **Figure 3: Zonal mean tropospheric ozone (ppbv) modelled (a) without and (b) with the nitrate scheme. The difference between (b) and (a) is shown in (c). The Lu21 lightning flash-rate parameterisation was used.**

OH is the controlling oxidant in the global atmosphere and governs the chemical lifetime of most anthropogenic and natural gases, for example CH₄ and CO. Concentration of OH in the troposphere is governed by a complex set of chemical reactions involving species such as tropospheric O₃, CH₄, CO, nonmethane VOCs and NO_x, as well as the amount of humidity and solar radiation (e.g., Naik et al., 2013). The nitrate aerosol mechanism is linked to some of these reactions (e.g., those involving HNO₃) which leads to changes tropospheric OH. The simulated zonal average tropospheric OH in Figure 4a shows high OH levels near the in the tropical lower troposphere, particularly near the surface within 10–30° N with values as high as (20–25) × 10⁵ molecules cm⁻³. The OH concentrations decline with height, but a secondary maximum in the tropical upper troposphere (at ~ 13 km) is apparent, likely linked to LNO_x emissions. The corresponding Figure 4b with nitrate indicates some decrease in OH, and this is more apparent in the difference plot in Figure 4c where there is a decrease in OH everywhere with the largest changes being as much as 1.3 × 10⁵ molecules cm⁻³ within 0–40° N in the Northern Hemisphere. Overall, there is a decline of 5.0% in the global tropospheric OH when nitrate is included in the model.

370



375 **Figure 4: Zonal mean tropospheric OH (× 10⁵ molecules cm⁻³) simulated (a) without and (b) with the nitrate scheme. The difference between (b) and (a) is shown in (c). The Lu21 lightning flash-rate parameterisation was used.**



As a consequence of the decrease in OH with nitrate in the model, the methane lifetime (τ_{CH_4}) with respect to loss by OH in the troposphere increases by 5% from 7.0 years, and on average the tropospheric CO goes up by 3.0% from the global average value of 78.1 ppbv, as compared to the simulation with no nitrate. On the other hand, there is a decrease in NO by 7.5% and that in NO₂ by 6.7%, owing to the swift removal of particulate nitrate from the atmosphere compared to gas phase nitrogen species. In Figure 5a, τ_{CH_4} plotted as a function of LNO_x for all simulations (Table 2) suggests that within the range of LNO_x considered, on average, τ_{CH_4} is greater by ~ 0.4 years when nitrate is included. This approximately equates to the increase in τ_{CH_4} as a result of per unit Tg N yr⁻¹ decrease in LNO_x (using the slopes of the linear best fit lines in Figure 5a).

The 1-sigma standard deviation uncertainty in τ_{CH_4} in Figure 5a (and in Table 2) calculated based on the 15 years of simulation is on average ± 0.027 years which is much smaller than the mean decrease of ~ 1.7 years within the range of LNO_x considered. In Figure 5b, the reduction in the ozone burden in the troposphere when using the nitrate scheme is almost uniform at 16.5 Tg O₃ across the LNO_x values considered, and this magnitude is comparable to about 13 Tg O₃ generated per unit Tg N yr⁻¹ of LNO_x. This result is perhaps somewhat contrary to that reported by Tost (2017) who deduced that the nitrate formation does not have important influence on the distribution of tropospheric ozone. The tropospheric O₃ burden obtained by Luhar et al. (2020, 2021) with an older version of UM-UKCA (without nitrate) that used the Lu21 scheme (giving an LNO_x of 6.6 – 6.9 Tg N yr⁻¹) was 304 – 308 Tg O₃, which is considerably lower than 348.8 Tg O₃ obtained from the corresponding present simulation NN_Lu. Notwithstanding the various differences between the two simulations (e.g. differences in prescribed emissions, updated model schemes and parameters, nudging etc.), one important reason for this difference is that the old version of UKCA StratTrop included the chemical reaction $HO_2 + NO \rightarrow HNO_3$ which acts as a significant sink of HO_x (OH, HO₂) in the upper troposphere, and thus reducing ozone. However, based on further studies (e.g., Mertens et al., 2022), it was determined that this reaction was not important and was omitted in later versions of StratTrop. The uncertainty in the ozone burden in Figure 5b (and in Table 2) is on average ± 2.9 Tg O₃, much smaller than the mean increase of ~ 70 Tg O₃ within the LNO_x range considered.

400

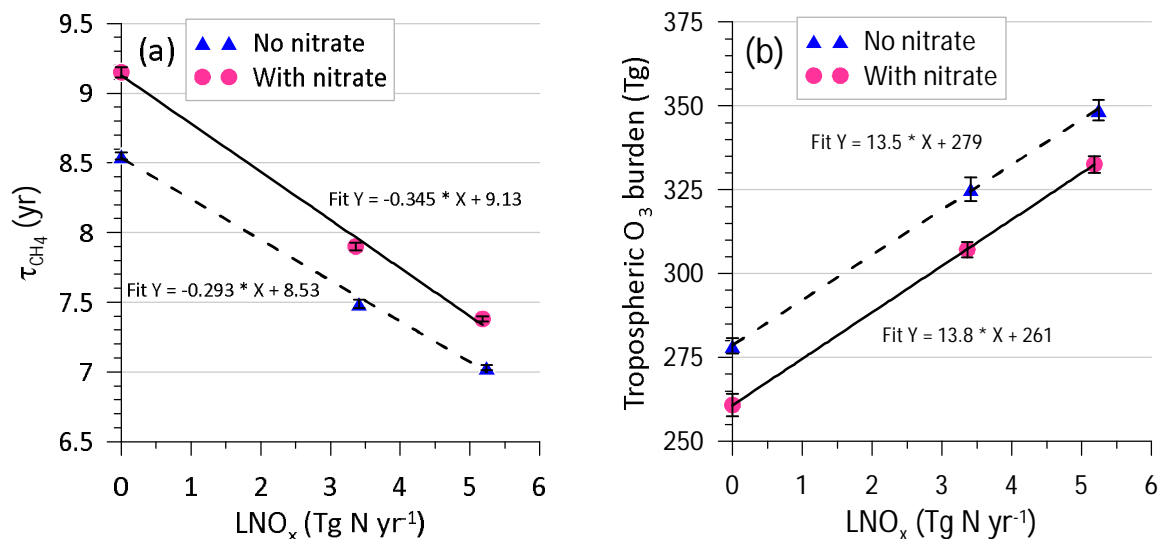
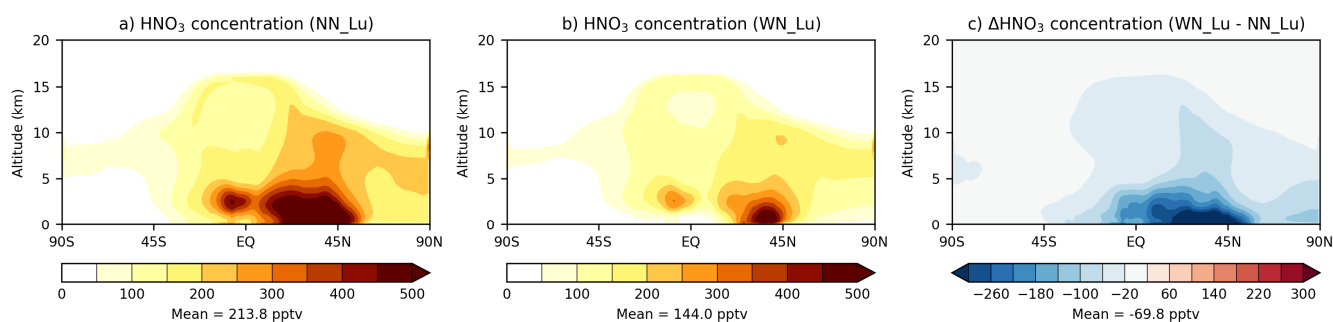


Figure 5: (a) Modelled methane lifetime (τ_{CH_4}) due to loss by tropospheric OH, as a function of lightning-generated NO_x, and (b) the same plot but for tropospheric O₃ burden. The lines are linear least squares fits and the error bars correspond to a 1-sigma standard deviation.

405

When nitrate aerosol is considered, there is a decrease in HNO₃ mixing ratio throughout the troposphere (Figure 6), mostly in the lower troposphere and between 0–45° N (where most of the surface NH₃ emissions are located), as part of the gas-phase HNO₃ is used up in the nitrate aerosol mechanism (following neutralisation by the uptake of ammonia). On average, this reduction is 33% compared to the no-nitrate value. The distribution of the reduction in Figure 6c is qualitatively very similar to that in NH₃, with the latter decreasing by 85% (plot not shown) compared to the no-nitrate case. We find that on average 1 Tg N yr⁻¹ of LNO_x emission results in a 11 pptv increase in tropospheric nitric acid mixing ratio with or without nitrate.

410



415

Figure 6: Zonal mean tropospheric HNO₃ (pptv) modelled (a) without and (b) with the nitrate scheme. The difference between (b) and (a) is shown in (c). The Lu21 lightning flash-rate parameterisation was used.



We have also looked at the gaseous nitrate radical (NO_3) (different from nitrate aerosol) and N_2O_5 (dinitrogen pentoxide) mixing ratios. The NO_3 radical has relatively low concentration but it is the controlling nighttime oxidant (the counterpart of OH in daytime) (Archer-Nicholls et al., 2023). It is generated by the reaction involving NO_2 and O_3 and reacts rapidly with unsaturated VOCs (e.g. isoprene and terpenes), thus affecting their atmospheric budgets as well as their degradation products (Khan et al., 2015). The NO_3 radical reacts further with NO_2 during nighttime to form N_2O_5 (dinitrogen pentoxide), another important nighttime species whose uptake onto aerosol removes NO_x from the atmosphere and produces nitric acid (Brown et al., 2006). We find that with the nitrate aerosol scheme, NO_3 radical is decreased by 11.5% overall from the tropospheric mean value of 0.5 pptv and, similarly, N_2O_5 goes down by 16.4% from the tropospheric mean value of 0.78 pptv.

4.3 Impact of LNO_x on aerosol mass concentration

Previous modelling studies have shown that lightning NO_x does lead to a significant increase in particulate nitrate concentrations (Tost, 2017). Jones et al. (2021) have presented results with nitrate aerosol that were obtained with the PR92 scheme, but without explicitly looking at sensitivity to lightning. Tost (2017) has investigated no- LNO_x and LNO_x (with the PR92 scheme) cases with nitrate included. We now investigate whether the changing of the LNO_x parameterisation (to Lu21) significantly impacts NO_3 concentrations. The three simulations (no- LNO_x , PR92 and Lu91) with and without nitrate also provide three amounts of global LNO_x against which the globally averaged parameter values can be plotted.

Ammonium nitrate aerosol is formed from HNO_3 condensation onto pre-existing aerosols, mainly thermodynamically stabilised by ammonium (NH_4^+). The modelled column annual-mean mass burdens of NH_4 (from both $(\text{NH}_4)_2\text{SO}_4$ and NH_4NO_3), fine NO_3 (from NH_4NO_3), coarse NO_3 (from both NaNO_3 and $\text{Ca}(\text{NO}_3)_2$) and SO_4 from the PR92 and Lu21 simulations and the differences between the two simulations (Lu21 – PR92) are shown in Figure 7 (top two rows). As fine NO_3 is associated with NH_4 , their spatial distributions are nearly the same, with relatively high burdens over land in the Northern Hemisphere, particularly over South Asia with values as high as $3 \text{ mg}[\text{N}] \text{ m}^{-2}$ and over East Asia / China with values as high as $2 \text{ mg}[\text{N}] \text{ m}^{-2}$. Over central North America, values as high as $1.1 \text{ mg}[\text{N}] \text{ m}^{-2}$ are predicted.

Moving from the PR92 to Lu21 scheme, there is a very small global mean increase ($\sim 1\%$) in both NH_4 and fine NO_3 burdens as LNO_x increases from 3.36 to $5.18 \text{ Tg N yr}^{-1}$. This increase is dominated by particle mass in the Aitken mode for NH_4 (68%) and accumulation mode for fine NO_3 (77%). There is a greater increase in the coarse NO_3 (as NaNO_3), at $\sim 4\%$.

However, the global difference plots in Figure 7 show considerable regional variations in the changes in aerosol burden, with the Lu21 scheme predicting larger fine nitrate concentrations over south-eastern China (by $90 \mu\text{g}[\text{N}] \text{ m}^{-2}$), North America and Central Africa (by $40 \mu\text{g}[\text{N}] \text{ m}^{-2}$), and western Europe (by $50 \mu\text{g}[\text{N}] \text{ m}^{-2}$). In contrast, the Lu21-predicted nitrate is lower over India (by as much as $100 \mu\text{g}[\text{N}] \text{ m}^{-2}$), north-east Asia and Eastern Europe. Very similar qualitative difference



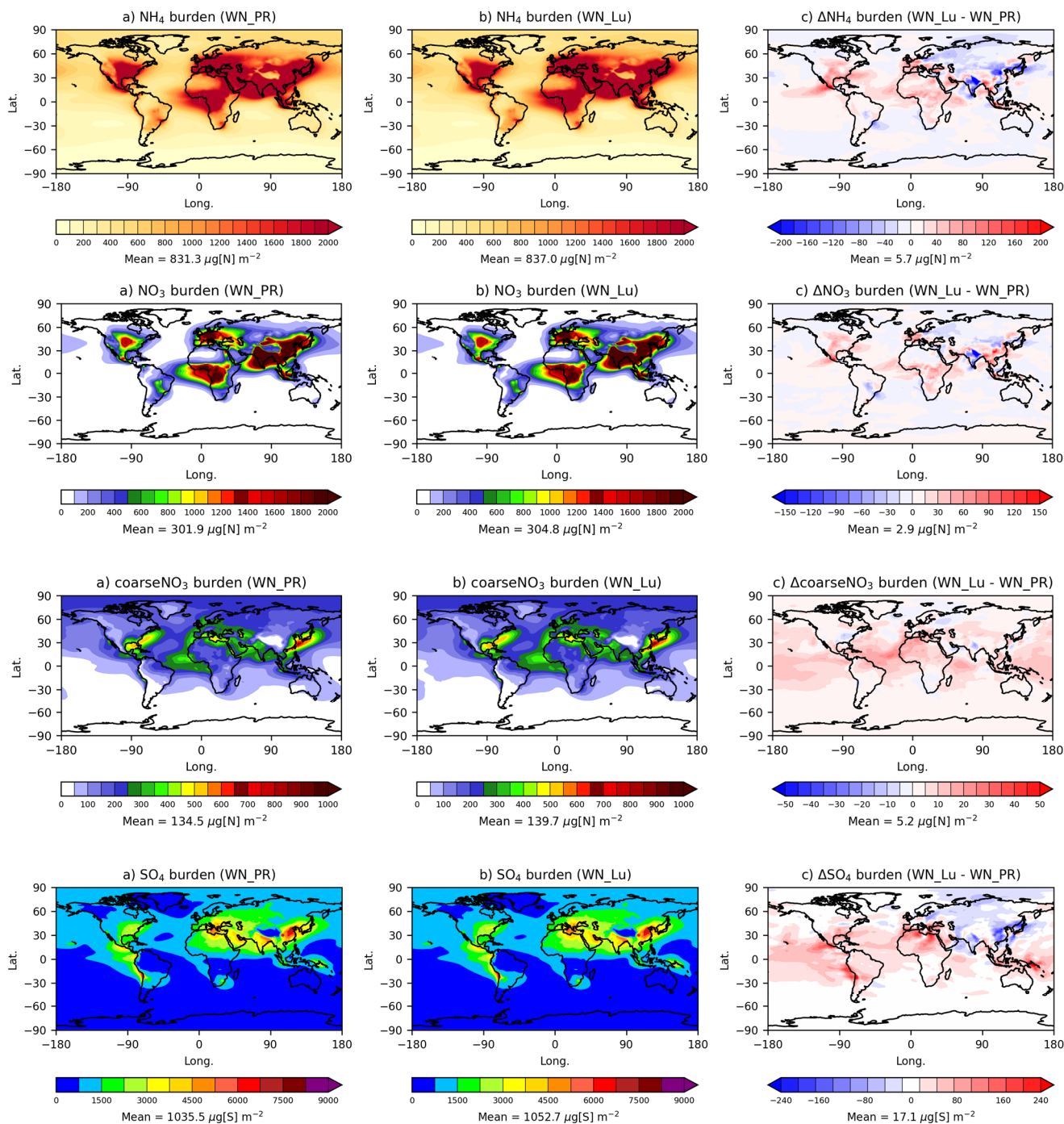
distribution is obtained for NH_4 . For coarse nitrate, there are increases over most of the globe, with larger magnitudes in the tropics (by $\sim 15 \mu\text{g}[\text{N}] \text{m}^{-2}$) compared to the PR92 scheme.

450 Sulfate aerosol is produced when OH oxidises SO_2 in the presence of water vapour to form H_2SO_4 which either nucleates or condenses on existing particles, depending upon its concentration. The distributions of SO_4 burden in Figure 7 (bottom panels) show a global increase of $\sim 1.7\%$ with the Lu21 scheme and this increase is dominated by the particles in the Aitken mode (55%) and accumulation mode (42%). There are relatively large increases ($\sim 70 \mu\text{g}[\text{S}] \text{m}^{-2}$) over most of the tropics, but burdens decrease over Russia, India, China, and north-east Asia.

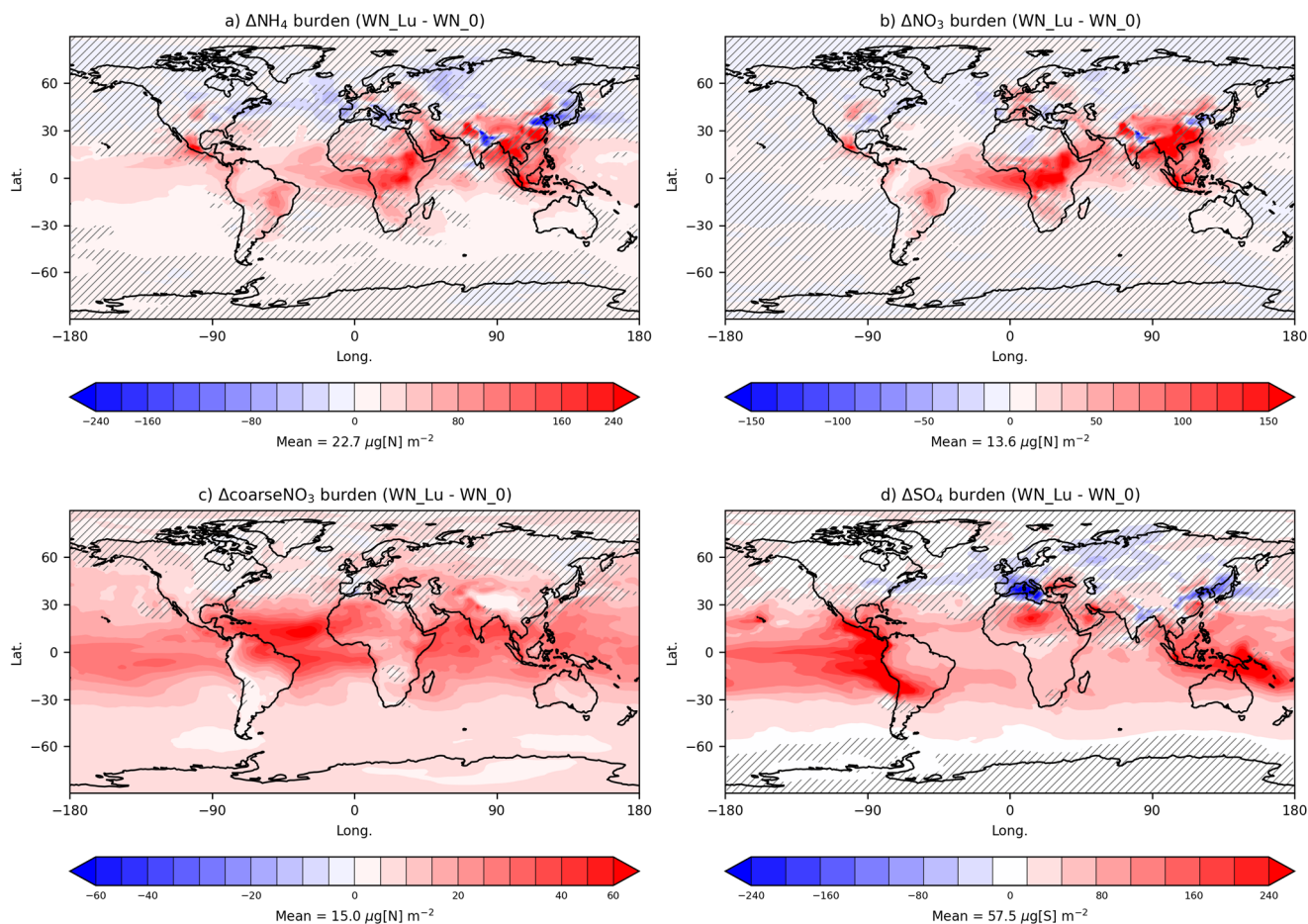
455 The tropospheric burdens of NH_4 , fine and coarse NO_3 , and SO_4 for the Lu21 scheme with nitrate are 0.43 Tg[N], 0.16 Tg[N], 0.07 Tg[N] and 0.54 Tg[S], respectively. These values can be compared with the global NH_4 , fine-mode NO_3 and SO_4 burdens of 0.13–0.58 Tg[N], 0.03–0.42 Tg[N], and 0.28–1.10 Tg[S], respectively, obtained from the AeroCom phase III model intercomparison study by Bian et al. (2017).

460 The above differences can be compared with those between the Lu21 scheme and when LNO_x is set to zero (which means the global LNO_x difference between the two cases is $5.18 \text{ Tg N yr}^{-1}$). Figure 8 is the same as Figure 7(right), except that the difference is between the Lu21 scheme and the no- LNO_x case. Hatched areas representing statistically insignificant difference (significance level less than 5%) are also plotted. On global average, there is a mean increase of 2.8% in NH_4 , 4.7% in fine NO_3 , 12% in coarse NO_3 , and 5.8% in SO_4 . This increase is dominated by particle mass in the Aitken mode for NH_4 (68%), accumulation mode for fine NO_3 (77%), coarse mode of NaNO_3 (73%) and Aitken mode for SO_4 (66%). Taken together Figure 7 and Figure 8 indicate that updating the LNO_x parameterisation from PR92 to Lu21 has a substantial impact on the LNO_x -mediated nitrate aerosol concentrations.

465



470 **Figure 7:** Annual-mean tropospheric mass burdens of NH_4 , fine NO_3 , coarse NO_3 , and SO_4 from the PR92 (left) and Lu21 (middle) simulations (both with nitrate) and the difference (right) between the two simulations.



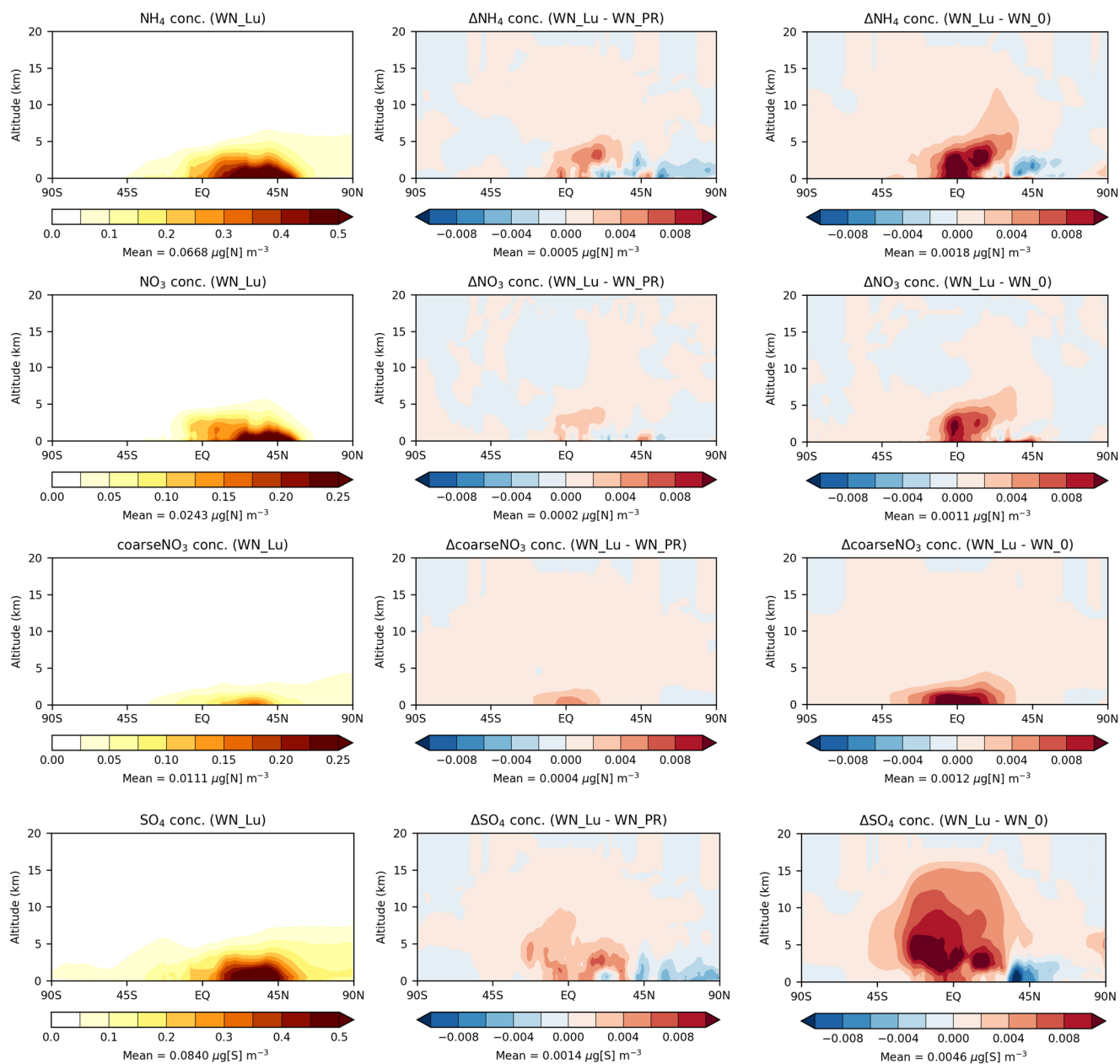
475 **Figure 8: Annual-mean tropospheric NH_4 , fine NO_3 , coarse NO_3 , and SO_4 burdens from the Lu21 and no-LNO_x simulations (both with nitrate) and the differences between the two simulations (Lu21 – no-LNO_x). The hatched areas represent statistically insignificant difference (significance level less than 5%).**

The zonal-mean vertical distributions of NH_4 , fine NO_3 , coarse NO_3 (related to sea salt and dust) and SO_4 mass concentrations from the Lu21 simulation (with nitrate) shown in Figure 9 (left) suggest that these species are mostly
 480 confined to the lower troposphere (as their precursors are emitted from sources close to the surface). High concentrations are predicted near the surface between the equator and 60°N which correspond to the locations of the main precursor emissions (i.e., NH_3 and NO_x). It is apparent that the vertical extent of fine NO_3 is limited because of the rapid wet removal of NH_3 gas from the atmosphere due to its high effective solubility, which in turn limits the vertical range to which NH_4NO_3 may establish by condensation. Conversely, near the surface over land regions NH_4NO_3 production is HNO_3 limited (Jones et al.,
 485 2021). NH_4 would reach a greater altitude than fine NO_3 , due to its long-lived association with SO_4 aerosol. The coarse NO_3



($\text{NaNO}_3 + \text{Ca}(\text{NO}_3)_2$) aerosol is also confined to near the surface as they are easily removed from the atmosphere by wet deposition and gravitational settling.

The differences between the Lu21 and PR92 simulations (Lu21 – PR92) (Figure 9, middle) indicate that with the Lu21 scheme there are noticeable increases in NH_4 and fine NO_3 mass concentrations around the equator below 4 km and an elevated maximum at an altitude of 3 km at around 15° N. While most of the LNO_x would be distributed vertically within the middle to upper troposphere in the tropics, NH_3 is mostly released at the surface between $0\text{--}60^\circ$ N, and thus these are the locations within the lower troposphere where LNO_x results in an optimal formation of NH_4 and fine NO_3 . This is clearer from the difference between the Lu21 and no- LNO_x simulations (Lu21 – no- LNO_x) (Figure 9, right) where the differences are much greater, but the qualitative shape of the difference patterns are very similar. This suggests that the differences in the distribution are governed by a balance between availability of LNO_x and NH_3 . There are areas of small decreases in the lower troposphere in the Northern Hemisphere beyond 40° N. With regards to the coarse NO_3 , the increases are mostly confined near the surface and symmetrically centred around the equator, which suggests that the differences in the distribution are dominated by LNO_x availability. The bottom plots in Figure 9 generally show increases in SO_4 with the Lu21 scheme throughout the troposphere between 40° S – 40° N and areas of decrease below 3 km beyond 40° N. There is an amplification of this behaviour when looking at the differences between the Lu21 case with the no- LNO_x case. The overall increase in SO_4 with the Lu21 scheme is possibly due to increase in tropospheric oxidants in response to increase in LNO_x .



505

Figure 9: Zonal mean tropospheric NH₄, fine NO₃, coarseNO₃, and SO₄ concentrations from the Lu21 simulation with nitrate (left), the difference between the Lu21 and PR92 simulations (Lu21 – PR92) (middle), and the difference between the Lu21 and no-LNO_x simulations (Lu21 – no-LNO_x) (right).

510



4.4 Impact of LNO_x on aerosol number concentration

In addition to the aerosol mass concentrations above, we can also examine zonal differences in prognostic aerosol number concentrations. Figure 10 presents the modelled zonal mean tropospheric aerosol number concentrations from the Lu21 simulation with nitrate (left), the difference between the Lu21 and PR92 simulations (Lu21 – PR92) (middle), and the difference between the Lu21 and no-LNO_x simulations (Lu21 – no-LNO_x) (right).
515

In Figure 10 (left), the nucleation mode (soluble) particles are the highest in number and are mostly located in the upper troposphere within 40° S – 40° N, followed by Aitken mode (soluble) particles with a maximum in the mid troposphere around the equator, and accumulation mode (soluble) particles in the lower troposphere between 30° S – 70° N. The coarse mode (soluble) particles (plot not shown) are the least in number and confined to very close to the surface due to their effective gravitational sedimentation, with more particles in the Southern Hemisphere than in the Northern Hemisphere
520 (probably due to a larger oceanic surface in the NH so as to cause a large sea salt particle number concentration).

The difference plots in Figure 10 (middle) show that the Lu21 scheme with its higher amount of LNO_x leads to a greater number concentration of nucleation mode particles (overall by about 3.6%) compared to the PR92 scheme, although there are regions, particularly near the tropopause between 30° S – 30° N, where the particle number concentration decreases with the Lu21 scheme. Both simulations include nitrate aerosol, but in the present scheme aerosol number concentrations are not modified explicitly by nitrate chemistry because of the assumption that NH₄ and NO₃ condense onto (and evaporates from) existing atmospheric aerosol rather than nucleating new particles. So, the changes in the number of nucleation mode particles in Figure 10 (middle) are likely due to an indirect impact of LNO_x changes on the oxidising capacity of the atmosphere (for example, via changes in OH and O₃), increases in which would generally lead to enhanced formation of new particles owing to faster oxidation rates of gas-phase sulfur to sulfate conversion as LNO_x is increased. (Enhancement of nucleation-mode particle numbers with lightning emissions in the upper troposphere was also predicted in the model simulations by Tost
530 (2017) which included nitrate.)

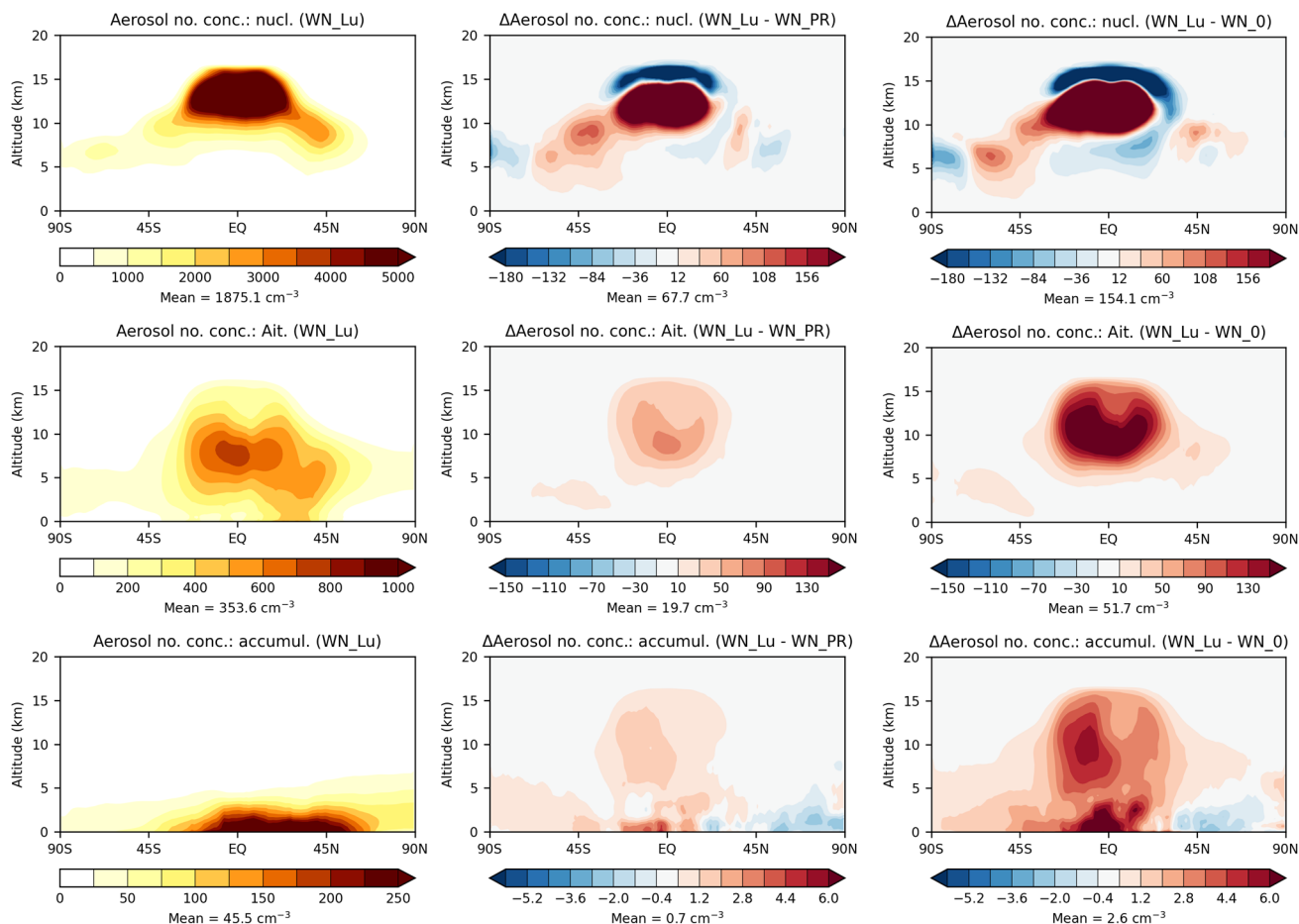
In Figure 10 (middle), there is an overall increase of 5.6% in the number of particles in the Aitken mode in the troposphere with the Lu21 scheme and this increase is centred in the middle of the troposphere (~ 8 km) within 30° S – 30° N. The particle number in the accumulation mode Figure 10 (bottom) is confined to lower troposphere and is impacted much less (~ 1.5%) by the change in the LNO_x scheme. There are negligible changes in the coarse mode and Aitken (insoluble) particle number concentrations with the changes in LNO_x amounts considered (plots not shown).
535

The differences in the particle numbers between the Lu21 scheme and the no-LNO_x case shown in Figure 10 (right) essentially show bigger increases but with qualitatively similar patterns – the increases in particle number in the nucleation, Aitken, and accumulation modes are 8.2%, 14.6% and 5.7%, respectively.
540



Thus, it is apparent from Figure 9 and Figure 10 that with the Lu21 scheme, with its 54% larger total LNO_x compared to the PR92 scheme, there is a rise in the aerosol mass concentration (of NH₄, fine NO₃, coarseNO₃ and SO₄) in the lower troposphere whereas there is an increase in the total aerosol number concentration, particularly in the nucleation and Aitken modes, in the mid to upper troposphere. The magnitudes of these increases are amplified when comparing the results from
545 the Lu21 scheme with the no-LNO_x case.

Wang et al. (2021) observed formation of new ultrafine particles during lightning events, resulting in large increases in nucleation and Aitken mode aerosols (by 18.9 and 5.6 times, respectively) coupled with ~12% intensification of nitrate aerosol signals (but it is not clear from their data if there were any nitrate signals in the nucleation mode). These increases are qualitatively consistent with the modelled differences with and without lightning shown in Figure 10. In our model,
550 nitrate does not participate in nucleation and the increases in particle numbers stem from LNO_x enhancing the oxidizing capacity of the troposphere and thus sulfate aerosol formation. Wang et al. (2021) point out that lightning channels may be conducive to an ion-induced nucleation process to generate new particles. Also, there is some evidence (e.g., Wang et al., 2020) that nitrate participates in nucleation directly. Note that any such direct new particle formation due to lightning or participation of nitrate in nucleation is not included in our model but may be considered in future versions of the UM as new
555 observations become available.



560 **Figure 10: Zonal mean tropospheric aerosol number concentrations from the Lu21 simulation with nitrate (left), the difference between the Lu21 and PR92 simulations (Lu21 – PR92) (middle), and the difference between the Lu21 and no-LNO_x simulations (Lu21 – no-LNO_x) (right).**

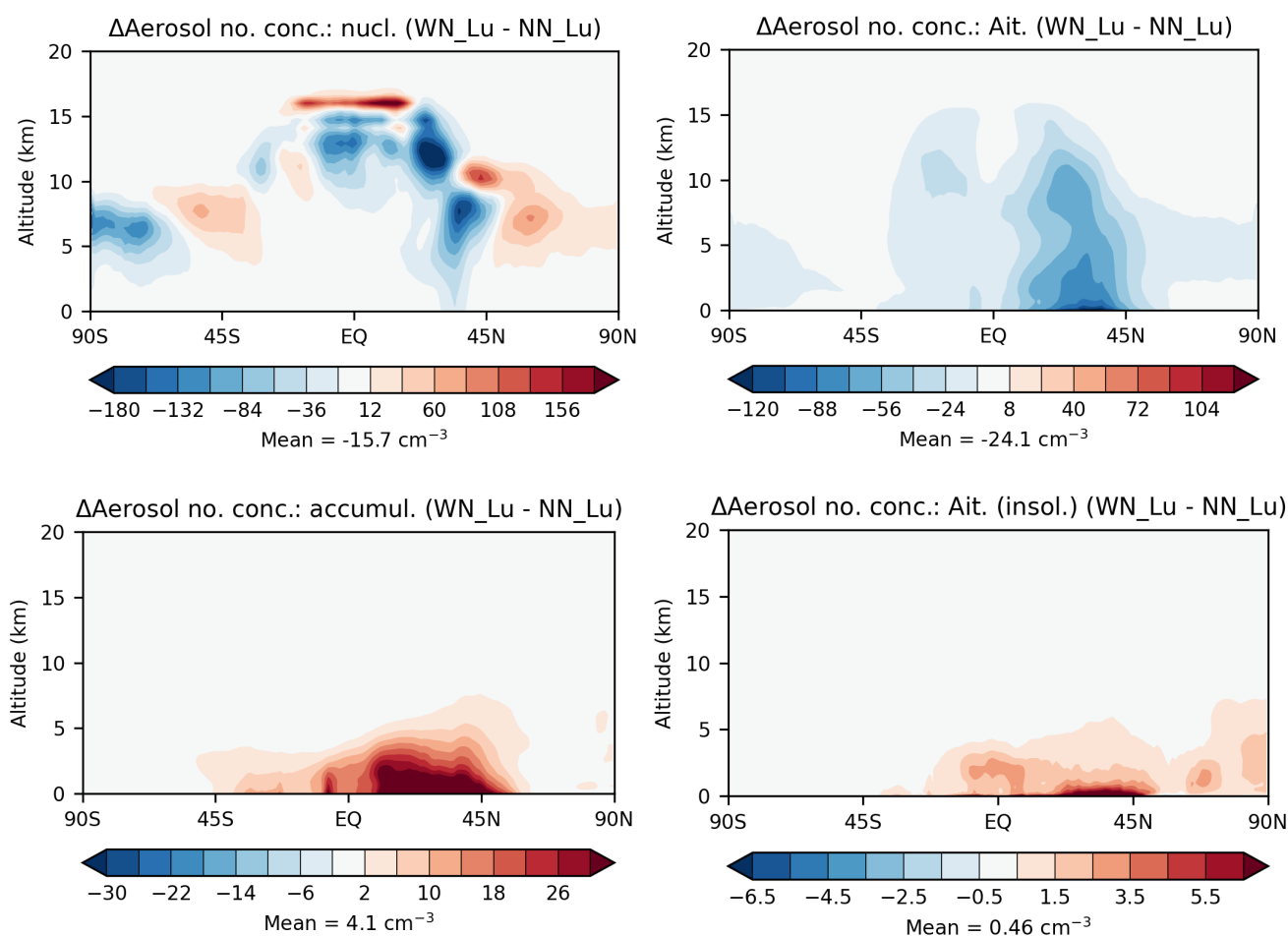
It is also instructive to present particle number concentrations without and with nitrate. In Figure 10, we already presented the modelled zonal mean tropospheric aerosol number concentrations from the Lu21 simulation with the nitrate scheme. Figure 11 presents the difference between this simulation and the same simulation without the nitrate scheme. There are regions of both increased and decreased nucleation mode (soluble) particle number concentrations from mid to upper troposphere with nitrate on, likely as a result of changes in oxidation rates of gas-phase sulfur to sulfate. But overall, there is a very small decrease of ~ 1% in nucleation model particle numbers with nitrate on. With nitrate on, there is a reduction in the Aitken mode particle number density (by 6.4% overall) throughout the troposphere, particularly between 10° – 50° N with higher concentrations in the lower troposphere. The probable reason for this is that condensational growth and altered

565



570 coagulation due the additional nitrate mass moves these particles to the accumulation mode. This is evident from the particle
 number distribution for the accumulation mode where there is a 10% enhancement in the particle number concentration with
 nitrate (mostly confined in the lower troposphere between 10° S – 50° N). Of all the modes, aerosols in the accumulation
 mode are of most importance as they have the greatest climate impact. They not only have the highest scattering efficiency,
 but they also have the longest atmospheric lifetime. They constitute the largest source of CCN.

575 The coarse mode aerosol number concentrations are much smaller (global tropospheric average = 0.16 cm⁻³), are confined to
 near the surface, and the inclusion of nitrate leads to an increase of 7.1% over the no-nitrate value.



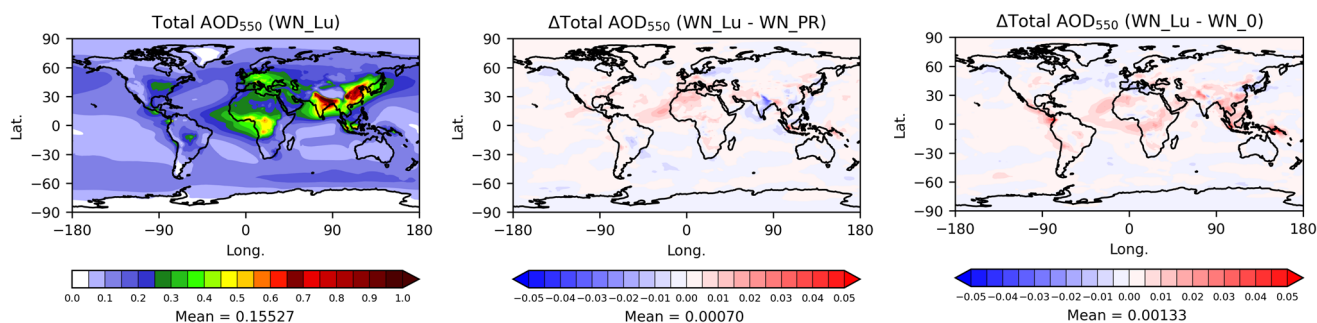
580 **Figure 11: Difference between the zonal mean tropospheric aerosol number concentrations in various aerosol modes from the Lu21 simulation with and without the nitrate scheme.**

We also looked at how tropospheric sulfate is impacted by the inclusion of nitrate, and this is presented in Supplement (S1).



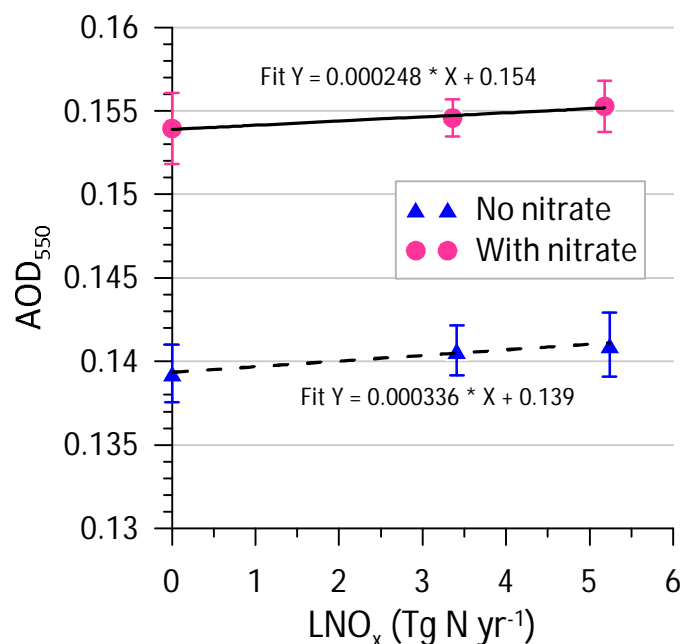
4.5 Impact of LNO_x on aerosol optical depth (AOD) and TOA radiation

585 As demonstrated earlier, significant differences in the size distribution of aerosol in the troposphere are caused by lightning. In conjunction with the inclusion of nitrate, this has ramifications for the aerosol extinction and cloud properties (Tost, 2017). In Figure 12 (left), we present the modelled column aerosol optical depth (AOD₅₅₀ at 550 nm wavelength) from the Lu21 simulation with nitrate. Large AODs over central Africa (biomass burning region), north-west Africa (dust emission region), and China and India (anthropogenic pollution emissions) are evident. These patterns are consistent with the 2003–
590 2012 mean MODIS (Collection 6) satellite AOD₅₅₀ data with a globally-averaged value of 0.162 (see Jones et al., 2021), which can be compared with the present model estimate of 0.155. The differences between the Lu21 and PR92 simulations (Lu21 – PR92) (Figure 12, middle) indicate that there is a very small (0.5%) overall increase in the global AOD₅₅₀ with the Lu21 scheme, but it is apparent there are larger differences regionally, for example an increase of 0.01–0.02 over north-western parts of Africa, western Europe, central Atlantic, and a decrease over India. The differences in AOD₅₅₀ between the
595 Lu21 scheme and the no-LNO_x case (both with nitrate) shown in Figure 12 (right) show, as expected, bigger increases (~ 1%).



600 **Figure 12: Annual-mean aerosol optical depth (AOD₅₅₀) from the Lu21 simulation with nitrate (left), the difference between the Lu21 and PR92 simulations (Lu21 – PR92) (middle), and the difference between the Lu21 and no-LNO_x simulations (Lu21 – no-LNO_x) (right).**

In Figure 13, globally averaged AOD₅₅₀ plotted as a function of LNO_x for all simulations suggests that within the range of LNO_x considered, on average, AOD₅₅₀ is greater by ~ 0.014 (about 11%) when nitrate is included (this difference is almost thrice as large as that obtained by Jones et al. (2021)). Based on the slopes of the linear least squares fits, the increase in
605 AOD₅₅₀ as a result of per unit Tg N yr⁻¹ increase in LNO_x is 2.1×10^{-4} with nitrate and 4.1×10^{-4} without nitrate. The 1-sigma standard deviation uncertainty bars in Figure 13 suggest that the mean increase in AOD₅₅₀ with LNO_x within the range of LNO_x considered is ~ 0.0015 which is comparable to or within the average AOD uncertainty of ~ ± 0.0017.



610 **Figure 13: Modelled globally averaged AOD₅₅₀ as a function of lightning-generated NO_x. The lines are linear least squares fits. The error bars correspond to a 1-sigma standard deviation.**

Lightning influences atmospheric radiation via changes in O₃ levels and methane lifetime, and through direct and indirect aerosol effects (e.g., Tost, 2017; Luhar et al., 2022). Figure 14 presents the modelled present-day all-sky annual-mean TOA net downward radiative flux (R_n^{TOA}), incorporating both shortwave and longwave components, as a function of LNO_x for both with and without nitrate cases. In the present model simulation, perturbation in this quality is akin to the total effective radiative forcing (ERF) (Bellouin et al., 2020). Although these are based on only three model runs, the slopes of the linear best fit lines in Figure 14 indicates that there is a rise of 36 mW m⁻² in R_n^{TOA} with a per Tg increase in N generated per year by lightning when nitrate is included in the model and it is 40 mW m⁻² without nitrate. (The latter is almost the same as 39.6 mW m⁻² (Tg N yr⁻¹)⁻¹ obtained by Luhar et al. (2022) using ACCESS-UKCA (an older version (v8.4) of UM-UKCA with somewhat different emission and model settings) without nitrate.) A positive change in R_n^{TOA} value suggests that that radiation is retained in the atmosphere, signifying warmer conditions. Since R_n^{TOA} increases with LNO_x, it implies that positive radiative feedback from an increase in ozone due to an increase in LNO_x dominates over negative radiative feedback resulting from reduction in methane lifetime and increase in aerosol concentration. This is true irrespective of whether nitrate is included or not. However, the change in R_n^{TOA} when nitrate is included is ~ -0.4 W m⁻² irrespective of LNO_x (Figure 14) which suggests that incorporation of nitrate in the model has a much bigger impact on R_n^{TOA} than any changes in LNO_x. Note that the difference of -0.4 W m⁻² is nearly twice as large as that obtained by Jones et al. (2021) and this is likely due to the various updates to UM that have happened moving from science configurations GA7.1 and GL7.0 to GA8.0 and GL9.0



(from UM vn11.8 to vn13.2), which include changes pertinent to aerosols, such as tuning of DMS emissions and cloud
 630 droplet spectral dispersion parameterisation, and near-surface drag improvements (Jones et al., 2022). As a comparison, in a
 regional model simulation study, Drugé et al. (2019) found that ammonium and nitrate aerosol caused a TOA direct radiative
 forcing of about -1.4 W m^{-2} under all sky conditions over Europe for the period 1979–2016. The uncertainty bars in Figure
 14 indicate that the increase in R_n^{TOA} with LNO_x within the range of LNO_x considered is $\sim 0.20 \text{ W m}^{-2}$ which can be
 compared within the average R_n^{TOA} uncertainty of $\sim \pm 0.125 \text{ W m}^{-2}$.

635

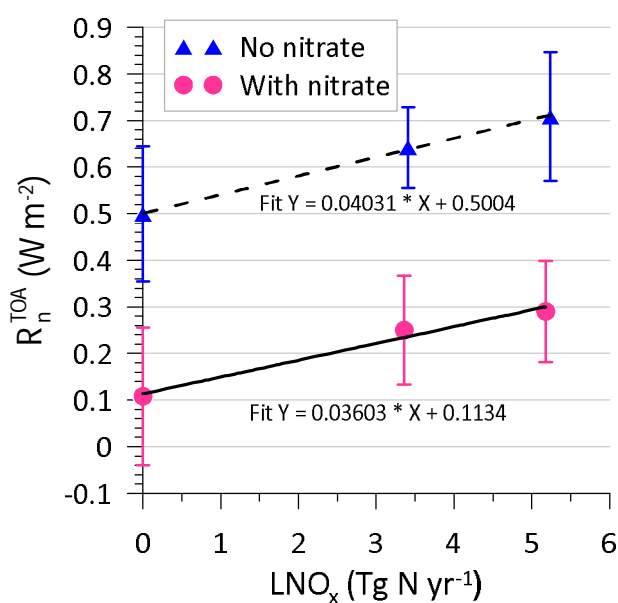


Figure 14: Modelled annual-mean top-of-atmosphere (TOA) net downward radiative flux, as a function of lightning-generated NO_x . The lines are linear least squares fits. The error bars correspond to a 1-sigma standard deviation.

640 It is clear that there are greater changes when nitrate is considered compared to changes caused by changes in LNO_x scheme.

We also examined the impact of nitrate on the modelled cloud droplet number concentration (CDNC) (see Supplement S2) and found that compared to the no- LNO_x case, there is a 3.1% increase in the mean tropospheric CDNC when LNO_x is considered (via the Lu21 scheme).

In this work, more complex flash-rate schemes can also be tried, for example the upward cloud ice flux based method of
 645 Finney et al. (2016) which is shown to perform better in the subtropics and part of the midlatitudes compared to the cloud-top height based schemes used here. However, we believe that the results on globally averaged atmospheric composition changes with LNO_x obtained here are not likely to change, but there could be regional impacts.



5 Conclusions

In this sensitivity focused study, we have essentially addressed two problems through the use of a global chemistry-climate model, UM-GA8.0-UKCA: 1) quantifying the impact of including nitrate aerosol on tropospheric composition, AOD and radiation, and 2) the dependency of these effects on lightning generated NO_x . The latter was explored by considering two empirical lightning flash-rate parameterisations: the PR92 scheme (Price and Rind, 1992) and the Lu21 scheme (Luhar et al., 2021), with the Lu21 scheme improving upon the underestimation of flash rate by the PR92 scheme over the ocean.

The amount of global LNO_x obtained from the Lu21 scheme was about 50% higher than that from the PR92 scheme (5.2 vs. 3.4 $\text{Tg}[\text{N}] \text{ yr}^{-1}$). This variation in LNO_x , together with the simulations with zero LNO_x , enabled an investigation of the change in globally averaged modelled atmospheric parameters as a (linear) function of LNO_x . We find that both nitrate aerosol and changes in LNO_x lead to significant changes in tropospheric composition and aerosol responses.

With the inclusion of nitrate aerosol, there was a decrease (of $\sim 4\text{--}5\%$) in the mean tropospheric O_3 volume mixing ratio, with the biggest reductions located in the mid to upper troposphere in the Northern Hemisphere. The methane lifetime increased by about 5% (~ 0.4 years) as the mean tropospheric OH concentration decreased. There were reductions in NH_3 , HNO_3 , gaseous nitrate radical and N_2O_5 mixing ratios. Aerosol size distribution also changed when nitrate aerosol is included. We found that there was a very small decrease of $\sim 1\%$ in aerosol number concentration in the nucleation mode, a reduction of $\sim 6.4\%$ in the Aitken mode, and an enhancement of $\sim 10\%$ in the accumulation mode. Of all the modes, aerosols in the accumulation mode are of most importance from climate impact, thus this change is significant. Inclusion of nitrate aerosol caused the mean AOD_{550} to increase by ~ 0.014 (11%) compared to when there was no nitrate aerosol in the model. However, the change in R_n^{TOA} when nitrate is included was $\sim -0.4 \text{ W m}^{-2}$ which suggests that incorporation of nitrate in the model has a much bigger impact on R_n^{TOA} than the variation considered in LNO_x . These results build on those presented in Jones et al. (2021) by determining the impact of nitrate aerosol on tropospheric composition, and will be useful for the development of UKESM2.

Comparing simulations with and without LNO_x emissions (corresponding to an LNO_x difference of 5.2 Tg N yr^{-1}), we show that the impact of LNO_x on global-mean atmospheric aerosol composition is an increase of 2.8% in NH_4 , 4.7% in fine NO_3 , 12% in coarse NO_3 , and 5.8% in SO_4 by mass. Moving from the PR92 to Lu21 scheme (with nitrate included), there was a very small global mean increase ($\sim 1\%$) in both NH_4 and fine NO_3 aerosol mass burdens. On the other hand, the increase in the coarse NO_3 was greater ($\sim 4\%$). This change in LNO_x scheme also increased the tropospheric SO_4 aerosol burden by $\sim 1.7\%$. These aerosol changes could be ascribed to particular aerosol modes, and they had considerable regional variations. These increases were dominated by the aerosol mass concentration in the lower troposphere. There was an increase of $\sim 3.6\%$ in the aerosol number concentration in the nucleation mode and an increase of $\sim 5.6\%$ in the Aitken mode, and these increases were dominated by increases in the mid to upper troposphere. A small decrease of $\sim 1.5\%$ was estimated in the accumulation mode with negligible changes in the other modes.



680 Compared to the PR92 scheme, the Lu21 scheme yielded a very small (0.5%) overall increase in the global AOD₅₅₀, but
there were significant differences regionally. The mean R_n^{TOA} increased by $\sim 0.07 \text{ W m}^{-2}$, which suggests that the positive
radiative feedback from an increase in ozone dominates over negative radiative feedback resulting from a reduction in
methane lifetime and increase in aerosol concentration as LNO_x is increased in the Lu21 scheme. In general, we find that the
magnitude of changes in gas-phase tropospheric composition as a result of changes in LNO_x going from the PR92 to Lu21
685 scheme (with a difference of 1.8 Tg N yr^{-1}) is roughly comparable to that caused by the inclusion of nitrate aerosol. But the
magnitude of changes in AOD and R_n^{TOA} are dominated by inclusion of nitrate.

The results presented here should also be considered in the context of uncertainty in the global amount of LNO_x. For
example, Schumann and Huntrieser (2007) report an uncertainty range of $2 - 8 \text{ Tg N yr}^{-1}$ in LNO_x. Thus, there would be
bigger variations in the values of the atmospheric parameters considered in this paper when considering this large
uncertainty range. Also, the default value of the HNO₃ uptake rate coefficient $\gamma = 0.193$ used in this study possibly represents
690 the upper end of efficiency of NH₄ and NO₃ aerosol production and thus its impact in the model. Further research is needed
to constrain this parameter better, exploring its potential dependence on aerosol composition, temperature, and relative
humidity. Also, any direct new particle formation (due to lightning or otherwise) is not yet explicitly included in the nitrate
scheme in UM-UKCA, which could be important – this may be considered in future versions of the UM. The results
695 obtained here on the degree of sensitivity to nitrate aerosol and LNO_x will be useful for further LNO_x and nitrate impacts
assessment in future UM studies.

In this paper, we have shown that simulating nitrate in GCMs is important for tropospheric composition, alongside radiation
and cloud droplet activation. We have also shown that simulating LNO_x production over the ocean (as in Lu21) produces a
tangible impact on regional aerosol concentrations at the surface, though the largest impacts are at higher altitudes where
700 LNO_x and NH₃ coexist. Our results could be used to infer the impact of changing lightning rates (and LNO_x emissions) on
nitrate concentrations under climate change.

Code availability

Owing to intellectual property rights restrictions, we cannot provide the source code or documentation papers for the UM.
The Met Office UM is available for use under licence. A number of research organisations and national meteorological
705 services use the UM in collaboration with the Met Office to undertake basic atmospheric process research, produce forecasts,
and develop the UM code. To apply for a licence, see <http://www.metoffice.gov.uk/research/modelling-systems/unified-model>
(Met Office, 2024). Geospatial figures were produced using Python 3.10.8 (<https://www.python.org>, last access: 27
February 2024) and Iris 2.4.0 (<https://scitools.org.uk>, last access: 27 February 2024).



Data availability

710 Output from the model suites used here is available on MASS tape archive and can be accessed upon request by obtaining a
login on U.K.'s environmental science data analysis facility at <http://www.jasmin.ac.uk>. The model suites used [UM@vn13.2](#)
and the suite IDs corresponding to the simulation names NN_0, NN_PR, NN_Lu, WN_0, WN_PR and WN_Lu used in this
paper are u-cx746, u-cx815, u-cx814, u-cx745, u-cx817 and u-cx819, respectively. The LIS/OTD lightning flash data
(V2.3.2015) were available from https://lightning.nsstc.nasa.gov/data/data_lis-otd-climatology.html (last access: 6 May
715 2021).

Author contributions

AKL designed the study, setup the modelling experiments, developed analysis scripts, analysed model output, and prepared
the paper with assistance from all co-authors. ACJ contributed to setting up the modelling experiments, advised on aerosol in
the model, oversaw the progress of simulations, and assisted with the development of analysis codes. JMW assisted with and
720 carried out part of the modelling work pertaining to lightning schemes.

Competing interests

The authors declare that they have no conflict of interest.

Acknowledgements

This work was supported by the CSIRO-UM Partnership Agreement project with the Met Office (CSIRO projects OD-
725 207701, OD-236140). Ashok Luhar acknowledges a travel award from the UM Partner Visiting Scientist Exchange (UNITE)
Program to visit the Met Office, Exeter, in June-July 20203 and thanks the UNITE Program manager Joao Teixeira for the
assistance provided with the application process and during the visit. We acknowledge Luke Roberts of the Met Office for
his assistance with setting up computational environment on JASMIN (U.K.'s storage and compute facility for
environmental sciences data analysis) to carry out model output analysis, and Martin Cope of CSIRO for his helpful
730 comments on this work.



References

- Archer-Nicholls, S., Allen, R., Abraham, N. L., Griffiths, P. T., and Archibald, A. T.: Large simulated future changes in the nitrate radical under the CMIP6 SSP scenarios: implications for oxidation chemistry, *Atmos. Chem. Phys.*, 23, 5801–5813, 735 <https://doi.org/10.5194/acp-23-5801-2023>, 2023.
- Archibald, A. T., O'Connor, F. M., Abraham, N. L., Archer-Nicholls, S., Chipperfield, M. P., Dalvi, et al.: Description and evaluation of the UKCA stratosphere–troposphere chemistry scheme (StratTrop vn 1.0) implemented in UKESM1, *Geosci. Model Dev.*, 13, 1223–1266, <https://doi.org/10.5194/gmd-13-1223-2020>, 2020.
- Bellouin, N., Rae, J., Jones, A., Johnson, C., Haywood, J., and Boucher, O.: Aerosol forcing in the Climate Model Intercomparison Project (CMIP5) simulations by HadGEM2-ES and the role of ammonium nitrate, *J. Geophys. Res.-Atmos.*, 116, D20206, <https://doi.org/10.1029/2011jd016074>, 2011.
- Bellouin, N., Mann, G. W., Woodhouse, M. T., Johnson, C., Carslaw, K. S., and Dalvi, M.: Impact of the modal aerosol scheme GLOMAP-mode on aerosol forcing in the Hadley Centre Global Environmental Model, *Atmos. Chem. Phys.*, 13, 3027–3044, <https://doi.org/10.5194/acp-13-3027-2013>, 2013.
- 745 Bian, H., Chin, M., Hauglustaine, D. A., Schulz, M., Myhre, G., Bauer, S. E., Lund, M. T., Karydis, V. A., Kucsera, T. L., Pan, X., Pozzer, A., Skeie, R. B., Steenrod, S. D., Sudo, K., Tsigaridis, K., Tsimpidi, A. P., and Tsyro, S. G.: Investigation of global particulate nitrate from the AeroCom phase III experiment, *Atmos. Chem. Phys.*, 17, 12911–12940, <https://doi.org/10.5194/acp-17-12911-2017>, 2017.
- Boccippio, D. J.: Lightning scaling relations revisited, *J. Atmos. Sci.*, 59, 1086–1104, [https://doi.org/10.1175/1520-0469\(2002\)059<1086:LSRR>2.0.CO;2](https://doi.org/10.1175/1520-0469(2002)059<1086:LSRR>2.0.CO;2), 2002.
- 750 Brown, S. S., Ryerson, T. B., Wollny, A. G., Brock, C. A., Peltier, R., Sullivan, A. P., Weber, R. J., Dube, W. P., Trainer, M., Meagher, J. F., Fehsenfeld, F. C., and Ravishankara, A. R.: Variability in nocturnal nitrogen oxide processing and its role in regional air quality, *Science*, 311, 67–70, <https://doi.org/10.1126/science.1120120>, 2006.
- Bucsela, E., Pickering, K. E., Allen, D., Holzworth, R., and Krotkov, N.: Midlatitude lightning NO_x production efficiency inferred from OMI and WLLN data. *J. Geophys. Res.-Atmos.*, 124, 13475–13497, <https://doi.org/10.1029/2019JD030561>, 2019.
- 755 Cecil, D. J., Buechler, D. E., and Blakeslee, R. J.: Gridded lightning climatology from TRMM-LIS and OTD: Dataset description, *Atmos. Res.*, 135–136, 404–414, <https://doi.org/10.1016/j.atmosres.2012.06.028>, 2014.
- Dahmann, K., Grewe, V., Ponater, M., and Matthes, S.: Quantifying the contributions of individual NO_x sources to the trend in ozone radiative forcing, *Atmos. Environ.*, 45, 2860–2868, <https://doi.org/10.1016/j.atmosenv.2011.02.071>, 2011.
- 760



- Drugé, T., Nabat, P., Mallet, M., and Somot, S.: Model simulation of ammonium and nitrate aerosols distribution in the Euro-Mediterranean region and their radiative and climatic effects over 1979–2016, *Atmos. Chem. Phys.*, 19, 3707–3731, <https://doi.org/10.5194/acp-19-3707-2019>, 2019.
- 765 Finlayson-Pitts, B. J. and Pitts, J. N.: *Chemistry of the Upper and Lower Atmosphere: Theory, Experiments and Applications*, Academic Press, San Diego, ISBN: 0-12-257060-x, 969 pages, 2000.
- Finney, D. L., Doherty, R. M., Wild, O., and Abraham, N. L.: The impact of lightning on tropospheric ozone chemistry using a new global lightning parametrisation, *Atmos. Chem. Phys.*, 16, 7507–7522, <https://doi.org/10.5194/acp-16-7507-2016>, 2016.
- Fuchs, N. A. and Sutugin, A. G.: *Highly Dispersed Aerosols*, Butterworth-Heinemann, Newton, Mass., USA, 105 pp., 1970.
- 770 Gordillo-Vázquez, F. J., Pérez-Invernón, F. J., Huntrieser, H., and Smith, A. K.: Comparison of six lightning parameterizations in CAM5 and the impact on global atmospheric chemistry, *Earth Space Sci.*, 6, 2317–2346, <https://doi.org/10.1029/2019EA000873>, 2019.
- Gregory, D. and Rowntree, P. R.: A mass flux convection scheme with representation of cloud ensemble characteristics and stability-dependent closure, *Mon. Weather Rev.*, 118, 1483–1506, [https://doi.org/10.1175/1520-0493\(1990\)118<1483:AMFCSW>2.0.CO;2](https://doi.org/10.1175/1520-0493(1990)118<1483:AMFCSW>2.0.CO;2), 1990.
- 775 Gressent, A., Sauvage, B., Cariolle, D., Evans, M., Leriche, M., Mari, C., and Thouret, V.: Modeling lightning-NO_x chemistry on a sub-grid scale in a global chemical transport model, *Atmos. Chem. Phys.*, 16, 5867–5889, <https://doi.org/10.5194/acp-16-5867-2016>, 2016.
- Griffiths, P. T., Murray, L. T., Zeng, G., Shin, Y. M., Abraham, N. L., Archibald, A. T., Deushi, M., Emmons, L. K., Galbally, I. E., Hassler, B., Horowitz, L. W., Keeble, J., Liu, J., Moeini, O., Naik, V., O'Connor, F. M., Oshima, N., Tarasick, D., Tilmes, S., Turnock, S. T., Wild, O., Young, P. J., and Zanis, P.: Tropospheric ozone in CMIP6 simulations, *Atmos. Chem. Phys.*, 21, 4187–4218, <https://doi.org/10.5194/acp-21-4187-2021>, 2021.
- 785 Hauglustaine, D. A., Balkanski, Y., and Schulz, M.: A global model simulation of present and future nitrate aerosols and their direct radiative forcing of climate, *Atmos. Chem. Phys.*, 14, 11031–11063, <https://doi.org/10.5194/acp-14-11031-2014>, 2014.
- Haywood, J. and Boucher, O.: Estimates of the direct and indirect radiative forcing due to tropospheric aerosols: A review, *Rev. Geophys.*, 38, 513–543, <https://doi.org/10.1029/1999RG000078>, 2000.
- Hoerling, M. P., Schaack, T. K., and Lenzen, A. J.: A global analysis of stratosphere-tropospheric exchange during northern winter, *Mon. Weather Rev.*, 121, 162–172, [https://doi.org/10.1175/1520-0493\(1993\)121%3C0162:AGAOSE%3E2.0.CO;2](https://doi.org/10.1175/1520-0493(1993)121%3C0162:AGAOSE%3E2.0.CO;2), 1993.
- 790



- Jones, A. C., Hill, A., Remy, S., Abraham, N. L., Dalvi, M., Hardacre, C., Hewitt, A. J., Johnson, B., Mulcahy, J. P., and Turnock, S. T.: Exploring the sensitivity of atmospheric nitrate concentrations to nitric acid uptake rate using the Met Office's Unified Model, *Atmos. Chem. Phys.*, 21, 15901–15927, <https://doi.org/10.5194/acp-21-15901-2021>, 2021.
- Jones, A. C., Hill, A., Hemmings, J., Lemaitre, P., Quérel, A., Ryder, C. L., and Woodward, S.: Below-cloud scavenging of aerosol by rain: a review of numerical modelling approaches and sensitivity simulations with mineral dust in the Met Office's Unified Model, *Atmos. Chem. Phys.*, 22, 11381–11407, <https://doi.org/10.5194/acp-22-11381-2022>, 2022.
- Khan, M. A. H., Cooke, M. C., Utembe, S. R., Archibald, A. T., Derwent, R. G., Xiao, P., Percival, C. J., Jenkin, M. E., Morris, W. C., and Shallcross, D. E.: Global modeling of the nitrate radical (NO₃) for present and pre-industrial scenarios, *Atmos. Res.*, 164–165, 347–357, <https://doi.org/10.1016/j.atmosres.2015.06.006>, 2015.
- 800 Labrador, L. J., von Kuhlmann, R., and Lawrence, M. G.: The effects of lightning-produced NO_x and its vertical distribution on atmospheric chemistry: sensitivity simulations with MATCH-MPIC, *Atmos. Chem. Phys.*, 5, 1815–1834, <https://doi.org/10.5194/acp-5-1815-2005>, 2005.
- Li, W. J. and Shao, L. Y.: Observation of nitrate coatings on atmospheric mineral dust particles, *Atmos. Chem. Phys.*, 9, 1863–1871, <https://doi.org/10.5194/acp-9-1863-2009>, 2009.
- 805 Luhar, A. K., Galbally, I. E., Woodhouse, M. T., and Thatcher, M.: An improved parameterisation of ozone dry deposition to the ocean and its impact in a global climate-chemistry model, *Atmos. Chem. Phys.*, 17, 3749–3767, <https://doi.org/10.5194/acp-17-3749-2017>, 2017.
- Luhar, A. K., Woodhouse, M. T., and Galbally, I. E.: A revised global ozone dry deposition estimate based on a new two-layer parameterisation for air–sea exchange and the multi-year MACC composition reanalysis, *Atmos. Chem. Phys.*, 18, 4329–4348, <https://doi.org/10.5194/acp-18-4329-2018>, 2018.
- 810 Luhar, A. K., Galbally, I. E., Woodhouse, M. T., and Abraham, N. L.: Assessing and improving cloud-height-based parameterisations of global lightning flash rate, and their impact on lightning-produced NO_x and tropospheric composition in a chemistry–climate model, *Atmos. Chem. Phys.*, 21, 7053–7082, <https://doi.org/10.5194/acp-21-7053-2021>, 2021.
- Luhar, A. K., Galbally, I. E., and Woodhouse, M. T.: Radiative impact of improved global parameterisations of oceanic dry deposition of ozone and lightning-generated NO_x, *Atmos. Chem. Phys.*, 22, 13013–13033, <https://doi.org/10.5194/acp-22-13013-2022>, 2022.
- Mann, G. W., Carslaw, K. S., Spracklen, D. V., Ridley, D. A., Manktelow, P. T., Chipperfield, M. P., Pickering, S. J., and Johnson, C. E.: Description and evaluation of GLOMAP-mode: a modal global aerosol microphysics model for the UKCA composition-climate model, *Geosci. Model Dev.*, 3, 519–551, <https://doi.org/10.5194/gmd-3-519-2010>, 2010.



- 820 Manners, J., Edwards, J. M., Hill, P., and Thelen, J.-C.: SOCRATES Technical Guide Suite Of Community RAdiative Transfer codes based on Edwards and Slingo, Met Office, UK, available at: <https://code.metoffice.gov.uk/trac/socrates> (last access: 26 February 2024), 2023.
- Marais, E. A., Jacob, D. J., Choi, S., Joiner, J., Belmonte-Rivas, M., Cohen, R. C., Beirle, S., Murray, L. T., Schiferl, L. D., Shah, V., and Jaeglé, L.: Nitrogen oxides in the global upper troposphere: interpreting cloud-sliced NO₂ observations from
825 the OMI satellite instrument, *Atmos. Chem. Phys.*, 18, 17017–17027, <https://doi.org/10.5194/acp-18-17017-2018>, 2018.
- Martin, R. V., Sauvage, B., Folkens, I., Sioris, C. E., Boone, C., Bernath, P., and Ziemke, J.: Space-based constraints on the production of nitric oxide by lightning, *J. Geophys. Res.*, 112, D09309, <https://doi.org/10.1029/2006JD007831>, 2007.
- Mertens, L. A., Winiberg, F. A. F., Allen, H. M., Sander, S. P., and Okumura, M.: Yields of HONO₂ and HOONO products from the reaction of HO₂ and NO using pulsed laser photolysis and mid-infrared cavity-ringdown spectroscopy, *J. Phys. Chem. A*, 126, 7342, <https://doi.org/10.1021/acs.jpca.2c04643>, 2022.
830
- Miyazaki, K., Eskes, H. J., Sudo, K., and Zhang, C.: Global lightning NO_x production estimated by an assimilation of multiple satellite data sets, *Atmos. Chem. Phys.*, 14, 3277–3305, <https://doi.org/10.5194/acp-14-3277-2014>, 2014.
- Mulcahy, J. P., Johnson, C., Jones, C. G., Povey, A. C., Scott, C. E., Sellar, A., Turnock, S. T., Woodhouse, M. T., Abraham, N. L., Andrews, M. B., Bellouin, N., Browse, J., Carslaw, K. S., Dalvi, M., Folberth, G. A., Glover, M., Grosvenor, D. P.,
835 Hardacre, C., Hill, R., Johnson, B., Jones, A., Kipling, Z., Mann, G., Mollard, J., O’Connor, F. M., Palmiéri, J., Reddington, C., Rumbold, S. T., Richardson, M., Schutgens, N. A. J., Stier, P., Stringer, M., Tang, Y., Walton, J., Woodward, S., and Yool, A.: Description and evaluation of aerosol in UKESM1 and HadGEM3-GC3.1 CMIP6 historical simulations, *Geosci. Model Dev.*, 13, 6383–6423, <https://doi.org/10.5194/gmd-13-6383-2020>, 2020.
- Murray, L. T.: Lightning NO_x and impacts on air quality, *Current Pollution Reports*, 2, 115–133,
840 <https://doi.org/10.1007/s40726-016-0031-7>, 2016.
- Naik, V., Voulgarakis, A., Fiore, A. M., Horowitz, L. W., Lamarque, J.-F., Lin, M., Prather, M. J., Young, P. J., Bergmann, D., Cameron-Smith, P. J., Cionni, I., Collins, W. J., Dalsøren, S. B., Doherty, R., Eyring, V., Faluvegi, G., Folberth, G. A., Josse, B., Lee, Y. H., MacKenzie, I. A., Nagashima, T., van Noije, T. P. C., Plummer, D. A., Righi, M., Rumbold, S. T., Skeie, R., Shindell, D. T., Stevenson, D. S., Strode, S., Sudo, K., Szopa, S., and Zeng, G.: Preindustrial to present-day
845 changes in tropospheric hydroxyl radical and methane lifetime from the Atmospheric Chemistry and Climate Model Intercomparison Project (ACCMIP), *Atmos. Chem. Phys.*, 13, 5277–5298, <https://doi.org/10.5194/acp-13-5277-2013>, 2013.
- Nault, B. A., Laughner, J. L., Wooldridge, P. J., Crouse, J. D., Dibb, J., Diskin, G., Peischl, J., Podolske, J. R., Pollack, I. B., Ryerson, T. B., Scheuer, E., Wennberg, P. O., and Cohen, R. C.: Lightning NO_x emissions: reconciling measured and modeled estimates with updated NO_x Chemistry, *Geophys. Res. Lett.*, 44, 9479–9488,
850 <https://doi.org/10.1002/2017GL074436>, 2017.



- Price, C. and Rind, D.: A simple lightning parameterization for calculating global lightning distributions, *J. Geophys. Res.-Atmos.*, 97, 9919–9933, <https://doi.org/10.1029/92JD00719>, 1992.
- Russo, M. R., Kerridge, B. J., Abraham, N. L., Keeble, J., Latter, B. G., Siddans, R., Weber, J., Griffiths, P. T., Pyle, J. A., and Archibald, A. T.: Seasonal, interannual and decadal variability of tropospheric ozone in the North Atlantic: comparison
855 of UM-UKCA and remote sensing observations for 2005–2018, *Atmos. Chem. Phys.*, 23, 6169–6196, <https://doi.org/10.5194/acp-23-6169-2023>, 2023.
- Schumann, U. and Huntrieser, H.: The global lightning-induced nitrogen oxides source, *Atmos. Chem. Phys.*, 7, 3823–3907, <https://doi.org/10.5194/acp-7-3823-2007>, 2007.
- Schwartz, S. E.: Mass transport considerations pertinent to aqueous phase reactions of gases in liquid-water clouds, in:
860 *Chemistry of Multiphase Atmospheric Systems*, edited by: Jaeschke, W., Springer, New York, 415–471, 1986.
- Stelson, A. W., Friedlander S. K., and Seinfeld, J. H.: A note on the equilibrium relationship between ammonia and nitric acid and particulate ammonium nitrate, *Atmospheric Environment*, 13, 369–371, [https://doi.org/10.1016/0004-6981\(79\)90293-2](https://doi.org/10.1016/0004-6981(79)90293-2), 1979.
- Szopa, S., Naik, V., Adhikary, B., Artaxo, P., Berntsen, T., Collins, W. D., Fuzzi, S., Gallardo, L., Kiendler Scharr, A.,
865 Klimont, Z., Liao, H., Unger, N., and Zanis, P.: Short-Lived Climate Forcers, in: *Climate Change 2021: The Physical Science Basis. Contribution of Working Group I to the Sixth Assessment Report of the Intergovernmental Panel on Climate Change*, edited by: Masson-Delmotte, V., Zhai, P., Pirani, A., Connors, S. L., Péan, C., Berger, S., Caud, N., Chen, Y., Goldfarb, L., Gomis, M. I., Huang, M., Leitzell, K., Lonnoy, E., Matthews, J. B. R., Maycock, T. K., Waterfield, T., Yelekçi, O., Yu, R., and Zhou, B., Cambridge University Press, Cambridge, UK and New York, NY, USA, 817–922,
870 <https://doi.org/10.1017/9781009157896.008>, 2021.
- Telford, P. J., Abraham, N. L., Archibald, A. T., Braesicke, P., Dalvi, M., Morgenstern, O., O'Connor, F. M., Richards, N. A. D., and Pyle, J. A.: Implementation of the Fast-JX Photolysis scheme (v6.4) into the UKCA component of the MetUM chemistry-climate model (v7.3), *Geosci. Model Dev.*, 6, 161–177, <https://doi.org/10.5194/gmd-6-161-2013>, 2013.
- Thornhill, G. D., Collins, W. J., Kramer, R. J., Olivíé, D., Skeie, R. B., O'Connor, F. M., Abraham, N. L., Checa-Garcia, R.,
875 Bauer, S. E., Deushi, M., Emmons, L. K., Forster, P. M., Horowitz, L. W., Johnson, B., Keeble, J., Lamarque, J.-F., Michou, M., Mills, M. J., Mulcahy, J. P., Myhre, G., Nabat, P., Naik, V., Oshima, N., Schulz, M., Smith, C. J., Takemura, T., Tilmes, S., Wu, T., Zeng, G., and Zhang, J.: Effective radiative forcing from emissions of reactive gases and aerosols – a multi-model comparison, *Atmos. Chem. Phys.*, 21, 853–874, <https://doi.org/10.5194/acp-21-853-2021>, 2021.
- Tost, H.: Chemistry–climate interactions of aerosol nitrate from lightning, *Atmos. Chem. Phys.*, 17, 1125–1142,
880 <https://doi.org/10.5194/acp-17-1125-2017>, 2017.



- Walters, D., Baran, A. J., Boutle, I., Brooks, M., Earnshaw, P., Edwards, J., Furtado, K., Hill, P., Lock, A., Manners, J., Morcrette, C., Mulcahy, J., Sanchez, C., Smith, C., Stratton, R., Tennant, W., Tomassini, L., Van Weverberg, K., Vosper, S., Willett, M., Browse, J., Bushell, A., Carslaw, K., Dalvi, M., Essery, R., Gedney, N., Hardiman, S., Johnson, B., Johnson, C., Jones, A., Jones, C., Mann, G., Milton, S., Rumbold, H., Sellar, A., Ujiie, M., Whittall, M., Williams, K., and Zerroukat, M.:
885 The Met Office Unified Model Global Atmosphere 7.0/7.1 and JULES Global Land 7.0 configurations, *Geosci. Model Dev.*,
12, 1909–1963, <https://doi.org/10.5194/gmd-12-1909-2019>, 2019.
- Wang, Q., Li, Z., Guo, J., Zhao, C., and Cribb, M.: The climate impact of aerosols on the lightning flash rate: is it detectable
from long-term measurements? *Atmos. Chem. Phys.*, 18, 12797–12816, <https://doi.org/10.5194/acp-18-12797-2018>, 2018.
- Wang, M., Kong, W., Marten, R., He, X.-C., Chen, D., Pfeifer, J., Heitto, A., Kontkanen, J., Dada, L., Kürten, A., Yli-Juuti,
890 T., Manninen, H. E., Amanatidis, S., Amorim, A., Baalbaki, R., Baccarini, A., Bell, D. M., Bertozzi, B., Bräkling, S., Brilke,
S., Murillo, L. C., Chiu, R., Chu, B., Menezes, L.-P. D., Duplissy, J., Finkenzeller, H., Carracedo, L. G., Granzin, M., Guida,
R., Hansel, A., Hofbauer, V., Krechmer, J., Lehtipalo, K., Lamkaddam, H., Lampimäki, M., Lee, C. P., Makhmutov, V.,
Marie, G., Mathot, S., Mauldin, R. L., Mentler, B., Müller, T., Onnela, A., Partoll, E., Petäjä, T., Philippov, M., Pospisilova,
V., Ranjithkumar, A., Rissanen, M., Rörup, B., Scholz, W., Shen, J., Simon, M., Sipilä, M., Steiner, G., Stolzenburg, D.,
895 Tham, Y. J., Tomé, A., Wagner, A. C., Wang, D. S., Wang, Y., Weber, S. K., Winkler, P. M., Wlasits, P. J., Wu, Y., Xiao,
M., Ye, Q., Zauner-Wieczorek, M., Zhou, X., Volkamer, R., Riipinen, I., Dommen, J., Curtius, J., Baltensperger, U.,
Kulmala, M., Worsnop, D. R., Kirkby, J., Seinfeld, J. H., El-Haddad, I., Flagan, R. C., and Donahue, N. M.: Rapid growth of
new atmospheric particles by nitric acid and ammonia condensation, *Nature*, 581, 184–189, <https://doi.org/10.1038/s41586-020-2270-4>, 2020.
- 900 Wang, H., Pei, Y., Yin, Y., Shen, L., Chen, K., Shi, Z., and Chen, J.: Observational evidence of lightning-generated ultrafine
aerosols, *Geophys. Res. Lett.*, 48, e2021GL093771, <https://doi.org/10.1029/2021GL093771>, 2021.
- Wilson, D. R. and Ballard, S. P.: A microphysically based precipitation scheme for the UK Meteorological Office Unified
Model, *Q. J. Roy. Meteorol. Soc.*, 125, 1607–1636, <https://doi.org/10.1002/qj.49712555707>, 1999.
- Wilson, D. R., Bushell, A. C., Kerr-Munslow, A. M., Price, J. D., and Morcrette, C. J.: PC2: A prognostic cloud fraction and
905 condensation scheme. I: Scheme description, *Q. J. Roy. Meteorol. Soc.*, 134, 2093–2107, <https://doi.org/10.1002/qj.333>,
2008.
- Woodward, S.: Modeling the atmospheric life cycle and radiative impact of mineral dust in the Hadley Centre climate
model, *J. Geophys. Res.-Atmos.*, 106, 18155–18166, <https://doi.org/10.1029/2000JD900795>, 2001.